Low-frequency target strength and abundance of shoaling Atlantic herring (Clupea harengus) in the Gulf of Maine during the Ocean Acoustic Waveguide Remote Sensing 2006 Experiment

Low-frequency target strength and abundance of shoaling Atlantic herring (*Clupea harengus*) in the Gulf of Maine during the Ocean Acoustic Waveguide Remote Sensing 2006 Experiment

Zheng Gong and Mark Andrews
Department of Electrical and Computer Engineering, Northeastern University, Boston, Massachusetts 02115

Srinivasan Jagannathan
Department of Mechanical Engineering, Massachusetts Institute of Technology, Cambridge, Massachusetts 02139

Ruben Patel
Institute of Marine Research, P.O. Box 1870, Nordnes, N-5817 Bergen, Norway

J. Michael Jech
Northeast Fisheries Science Center, 166 Water Street, Woods Hole, Massachusetts 02543

Nicholas C. Makris
Department of Mechanical Engineering, Massachusetts Institute of Technology, Cambridge, Massachusetts 02139

Purnima Ratilal
Department of Electrical and Computer Engineering, Northeastern University, Boston, Massachusetts 02115

(Received 30 January 2009; revised 21 October 2009; accepted 26 October 2009)

The low-frequency target strength of shoaling Atlantic herring (*Clupea harengus*) in the Gulf of Maine during Autumn 2006 spawning season is estimated from experimental data acquired simultaneously at multiple frequencies in the 300–1200 Hz range using (1) a low-frequency ocean acoustic waveguide remote sensing (OAWRS) system, (2) areal population density calibration with several conventional fish finding sonar (CFFS) systems, and (3) low-frequency transmission loss measurements. The OAWRS system's instantaneous imaging diameter of 100 km and regular updating enabled unaliased monitoring of fish populations over ecosystem scales including shoals of Atlantic herring containing hundreds of millions of individuals, as confirmed by concurrent trawl and CFFS sampling. High spatial-temporal coregistration was found between herring shoals imaged by OAWRS and concurrent CFFS line-transects, which also provided fish depth distributions. The mean scattering cross-section of an individual shoaling herring is found to consistently exhibit a strong, roughly 20 dB/octave roll-off with decreasing frequency in the range of the OAWRS survey over all days of the roughly 2-week experiment, consistent with the steep roll-offs expected for sub-resonance scattering from fish with air-filled swimbladders.
 [DOI: 10.1121/1.3268595]

PACS number(s): 43.30.Sf, 43.30.Pc, 43.30.Vh [RCG] Pages: 104–123

I. INTRODUCTION

To study the scattering characteristics, abundance and diurnal behavior of Atlantic herring (*Clupea harengus*), the most abundant fish species in and around Georges Bank during their Autumn spawning season,[1] an experiment using ocean acoustic waveguide remote sensing (OAWRS) was conducted in the Gulf of Maine from September 19 to October 6, 2006, concentrating on areas where herring shoals were most likely to form (Fig. 1). The experiment, known as OAWRS 2006, was conducted in conjunction with the U.S. National Marine Fisheries Service Annual Atlantic Herring Acoustic Survey of the Gulf of Maine and Georges Bank. Fish populations were instantaneously imaged over a 100 km diameter area by a mobile OAWRS system[2] with minute-to-minute updates to form wide-area movies of fish activity over many diurnal cycles, demonstrating the capacity of OAWRS to instantaneously image fish populations over wide areas in complex continental-shelf environments with highly variable bathymetry and oceanography. Shoals imaged by OAWRS typically comprised tens to hundreds of millions of individuals and stretched for many kilometers along the northern flank of Georges Bank. Concurrent conventional fish finding sonar (CFFS) surveys showed high spatio-temporal coregistration with fish shoals imaged by OAWRS and provided local areal population densities, as well as depth and length distributions of the fish populations. Concurrent trawl sampling, which showed Atlantic herring to be the overwhelmingly predominant species comprising the large shoals,[2,3] enabled onsite species identification and direct biological measurements of parameters such as fish length, swimbladder geometry, stomach content, and sexual development.

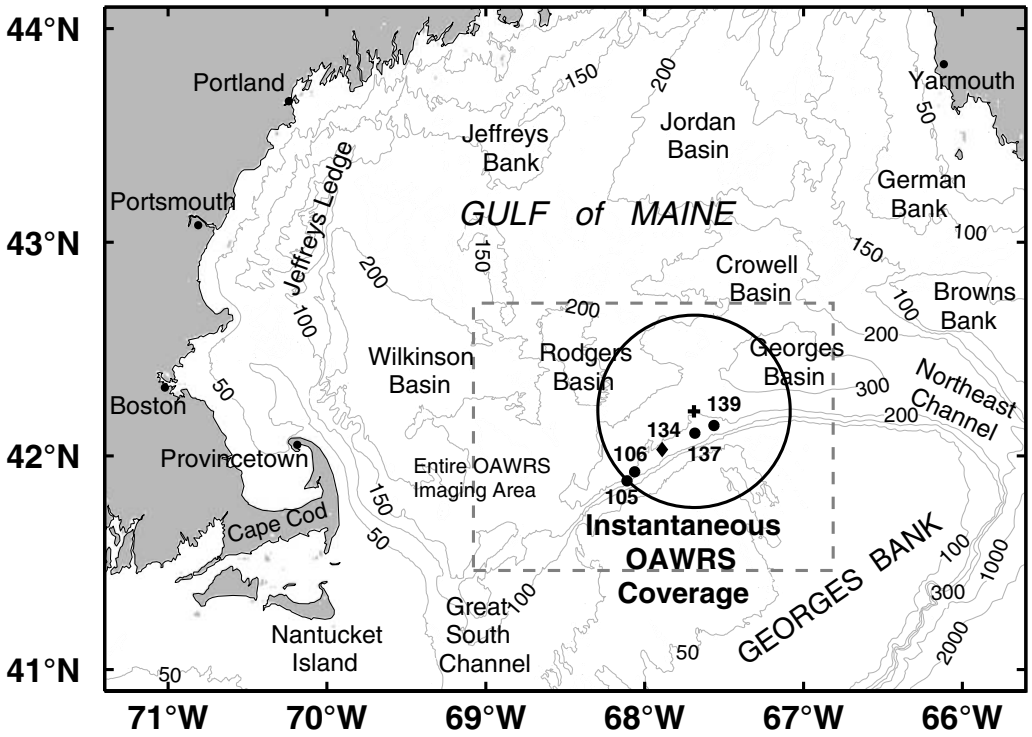

FIG. 1. Location of OAWRS 2006 experiment on the northern flank of Georges Bank in the Gulf of Maine. Plus indicates location of moored OAWRS source array deployed on Oct 1–3 at 42.2089N, 67.6892W, the coordinate origin for all OAWRS images in this paper. Circle shows typical area imaged by OAWRS, 100 km diameter and wider than Cape Cod, in 70 s. Geographic locations of trawls deployed by NOAA FRV *Delaware II* are overlain. Dots indicate trawls where herring were predominant species. In contrast, diamond indicates a trawl where silver hake and squids dominated. The gray dashed box bounds the area of OAWRS imaging during the OAWRS 2006 experiment.

Together with long-range transmission loss measurements, concurrent CFFS, and trawl data, the OAWRS imagery enabled (1) estimates of herring target strength to be made at low frequencies (300–1200 Hz) from which physical scattering mechanisms may be inferred, (2) herring spatial distributions and abundance to be estimated over ecosystem scales, and (3) regular diurnal patterns in herring behavior to be determined during the Autumn spawning season on Georges Bank.[3,4]

The mean scattering cross-section of an individual shoaling herring is found to consistently exhibit a strong, roughly 20 dB/octave roll-off with decreasing frequency in the range of the OAWRS survey over many measurement days, consistent with the steep roll-off expected for subresonance scattering from fish with air-filled swimbladders. These findings suggest that OAWRS can provide valuable evidence for remote species classification over wide areas since significant variations in the frequency dependence of target strength are expected across species due to differences in resonance. This is because the dominant source of acoustic scattering at low and mid-frequencies (less than 10 kHz) is the air-filled swimbladder for fish that have swimbladders.[5] Resonance frequencies depend on swimbladder volume, shape, ambient pressure, and the effect of surrounding tissues.[6,7] For many fish species of economic importance in the size ranging from 10 to 50 cm, resonances are expected to range from several hundreds of hertz to a few kilohertz.[6–9] Previous experimental investigation of resonance have been limited to small scale tank measurements with individual fish out of their natural environment or highly localized measurements made *in situ* with sources of rapid power roll-off below 1.7 kHz.[7,10,11]

The population that spawns on the northern flank of Georges Bank (Fig. 1) is the largest herring stock in the Gulf of Maine, and has both ecological and economic importance.[1] It has been surveyed annually by the U.S. National Marine Fisheries Service for roughly 1 decade during the Autumn spawning season.[12–14] Current estimates of the Georges Bank herring stock varies from 500 000 to 1×10^6 tons based on acoustic surveys and other assessment methods,[14] respectively. The National Marine Fisheries Service acoustic survey employs highly localized CFFS measurements along widely spaced line-transects, roughly 20–30 km apart,[14] trawl sampling at selected locations, and takes roughly 1 week to cover the northern flank of Georges Bank from east to west. As a result, annual stock estimates may be highly aliased in both time and space. One of the primary goals for OAWRS 2006 is to provide images of fish populations over the vast areas they inhabit that are unaliased in both space and time[2] so that more reliable abundance estimates may be obtained.

II. MULTI-SENSOR EXPERIMENT DESIGN AND RESOURCES

The OAWRS 2006 experiment was designed to coincide with the National Marine Fisheries Service annual herring survey of Georges Bank. It was conducted with four research vessels (RVs) that employed a suite of acoustic imaging sensors, several oceanographic monitoring systems, and trawls

TABLE I. OAWRS receiving array 3-dB angular resolution $\beta(\phi)$ at broadside $\phi=0$ and endfire $\phi=\pi/2$, and aperture length L as a function of imaging frequency f_c. A Hanning spatial window is applied in the beamforming.

f_c (Hz)	L (m)	$\beta(\phi=0)/\beta(\phi=\pi/2)$ (deg)
415	94.5	3.15/31.4
735	47.25	3.56/33.3
950	47.25	2.75/29.3
1125	23.625	4.65/38.1

for species identification. The OAWRS vertical source array and towed horizontal receiving array were separately deployed from two medium sized UNOL vessels, RV *Endeavor* and RV *Oceanus* respectively, for bistatic measurement of echo returns. The instantaneous areal coverage of the OAWRS system in a single transmission is shown in Fig. 1. The vertical source array transmitted a suite of individual Tukey-windowed linear frequency modulated (LFM) pulses of 1 s duration and 50 Hz bandwidth centered at a suite of frequencies with a repetition interval of 150 s for each center frequency.[15] Broadband LFM pulses centered at 415 and 735 Hz were transmitted seconds apart, then after 75 s those centered at 950 and 1125 Hz were transmitted seconds apart, and the process was repeated. Transmissions radiated with azimuthal symmetry about the OAWRS source array, for which more information is available in Ref. 16, with source level continuously monitored with two desensitized hydrophones deployed from RV *Endeavor*. Scattered returns were acquired with a horizontal receiving array, the ONR five-octave research array, towed by RV *Oceanus* along designated tracks. The multiple nested sub-apertures of the array span 50–3750 Hz frequency range. Returns measured within each linear section of the array are processed by beamforming and matched filtering with angular resolution shown in Table I. The receiving array also contained one desensitized hydrophone which was used to measure transmitted signals from the source array for transmission loss and source level calibrations. Two calibrated acoustic targets made of air-filled rubber hose,[17] approximately 30 m long and 7 cm in diameter with known scattering properties,[18] were vertically deployed at selected locations to enable accurate charting of scattered returns in both range and azimuth. One of the targets was moored with lower end 5 m off the seafloor and the other was centered at 140 m in waters 200 m deep.

Over the course of the OAWRS 2006 experiment, more than 3000 wide-area images of the ocean environment were acquired by the OAWRS system for each of the four LFM center frequencies leading to more than 12 000 images in total. Similarly, more than 12 000 transmission loss measurements were made over the survey area to calibrate our transmission loss model. The length of each RV *Oceanus* towed array track was typically 15 km. With a nominal tow speed of 2 m s^{-1} for the receiver ship, a total of roughly 75 images of the ocean environment were generated per frequency along each track. Minute-to-minute updates of the OAWRS imagery made it possible to closely monitor herring activity over wide areas and observe patterns of spatial distribution evolve over the course of each day. The inherent left-right

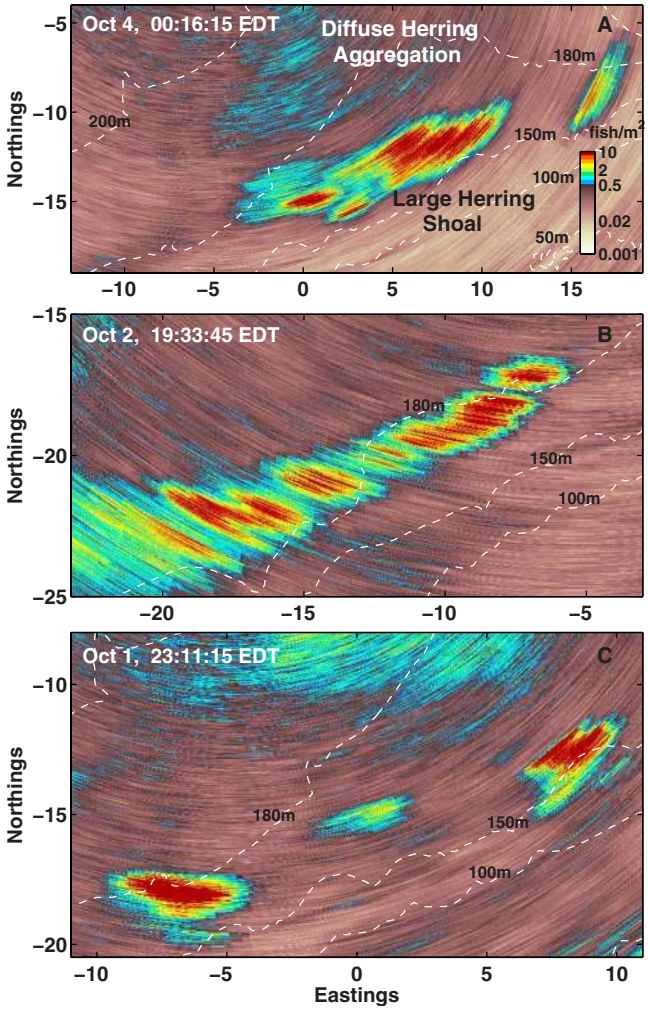

FIG. 2. (Color online) [(A)–(C)] OAWRS images of areal fish density zoomed-in around massive herring shoals, with densities exceeding 10 fish m^{-2} in population centers. Measured during evening to midnight hours of October 4, 2, and 1, respectively. (A) The total population of herring in the large dense shoal is roughly 170×10^6, and that in the diffuse cloud outside the large shoal is roughly 70×10^6. Imaged shoal populations of herring are approximately 86×10^6 and 70×10^6 respectively for (B) and (C). Uncertainty in the abundance estimate is 17–20%. Note that the figures are plotted on different scales, and the coordinate origin is the source location shown in Fig. 1.

ambiguity about the horizontal line-array's axis in the OAWRS images were resolved mainly by varying receiver ship heading, sometimes only slightly for several transmissions by what we call a "Crazy Ivan" for immediate results, as well as ship position. These approaches for ambiguity resolution are described in Refs. 19–21.

Examples of the massive fish shoals instantaneously imaged by OAWRS near Georges Bank are shown in Fig. 2. The massive shoal imaged during midnight hours of October 4 within the 150–180 m bathymetric contour in Fig. 2(A), for example, extends 15×5 km^2 and comprises roughly 170×10^6 fish distributed about several population centers. The area occupied by this shoal is approximately equal to that of Manhattan Island in New York. The fish population in the diffuse cloud region to the north is comprised of over 70×10^6 individuals.

Concurrent localized imaging of fish aggregations at OAWRS-directed locations was conducted by two other re-

TABLE II. Conventional fish finding sonars, SIMRAD EK60 and EK500 specifications. The angular 3-dB beamwidth is denoted by β, the pulse duration by PD, and repetition rate by RR. The resolution diameter, Res, is calculated for 200 m water depth.

Sensor	f (kHz)	β (deg)	Res (m)	PD (ms)	RR (s^{-1})
EK60	38				
	120	7	24	1	1
	200				
EK500	18	11	39	2	
	38	12	42	1	0.5
	120	7	24	1	

search vessels, the RV *Hugh Sharp* and the NOAA FRV *Delaware II*, using two downward-directed CFFS systems, the SIMRAD EK60 and EK500 echosounders, respectively. Both the EK60 and EK500 echosounders insonify the water column directly beneath the survey vessel simultaneously at three frequencies to provide the local depth dependence of dominant fish layers within their instantaneous resolution footprints, of between 24–50 m diameter, and estimates of volumetric and areal fish population densities. Specifications of these two echosounders appear in Table II. A Reson 7125 Seabat multi-beam sonar (400 kHz) system was also deployed from RV *Hugh Sharp* with an angular swath of 128°. It was useful in providing detailed three-dimensional morphology of smaller fish groups located in the mid-water column.[22] A high-speed rope trawl[23] deployed by NOAA FRV *Delaware II* enabled species identification[14] at OAWRS-directed locations.

Physical oceanography was monitored by sampling water-column temperature and salinity with expendable bathythermographs (XBTs) and conductivity-temperature-depth (CTD) sensors at regular hourly intervals from all four research vessels. The water-column sound speed profile was found to be relatively constant in space and time over the 2006 OAWRS survey, as shown by the compilation of over roughly 200 samples taken during the experiment in Fig. 3. No mesoscale oceanographic features such as eddies were found or expected. The small fluctuations about the mean profile are due to mild internal wave activity that causes well-understood short-term Gaussian field fluctuations in acoustic transmission that have an intensity standard deviation that can be reduced to a small fraction of the mean by stationary averaging.[24–26] An instrumented tow cable was also deployed from the RV *Hugh Sharp* to provide continuous measurement of temperature. This oceanographic information was used to carefully update horizontal locations and depths of the OAWRS source (typically centered at 60–70 m) and receiving arrays (centered at 105 m) (Ref. 15) to optimize OAWRS imaging of fish groups. Decisions were often based on the outputs of the range-dependent acoustic model (RAM), based on the parabolic equation, for multimodal waveguide transmission loss in the range-dependent Georges Bank environment with the hourly sound speed profile updates and known bathymetry.[27]

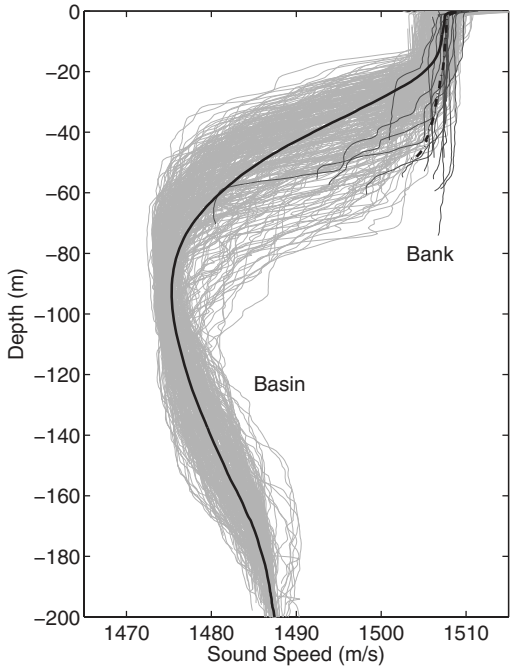

FIG. 3. Profiles of water-column sound speed from XBT and CTD measurements made from all four research vessels on the Northern Flank of Georges Bank and Georges Basin during OAWRS 2006.

III. DATA PROCESSING AND ANALYSIS

A. Generating instantaneous wide-area OAWRS images of the ocean environment

Wide-area images of instantaneous scattered intensity spanning 100 km in diameter were generated in near real-time for every broadband transmission centered at each of the four frequencies, f_c=415, 735, 950, and 1125 Hz. For each transmission, the pressure data on the receiving array were first beamformed to determine the azimuth of the arrivals, then matched filtered with the source signal, and charted in range using two-way travel time.[19–21] Each image was then mapped onto geographic space using the GPS latitude and longitude information of the source and receiving array. A nominal sound speed of 1475 m/s that minimizes charting errors was used to convert the travel-time of the signal to range.[21,28] The range resolution $\Delta\rho$ of the OAWRS system is approximately 15 m after matched-filtering, and the azimuthal resolution $\beta(\phi, f_c)$ associated with each frequency band both at broadside and endfire is tabulated in Table I. A Hanning spatial window was applied in the beamforming to reduce sidelobe levels by more than 30 dB from the main lobe. A detailed explanation of the image formation process is provided in Refs. 2, 20, and 21.

A standard procedure of averaging three consecutive instantaneous OAWRS images and two adjacent range cells is used for all OAWRS images presented here. This leads to an experimentally determined standard deviation in log-intensity of roughly 1.5 dB,[3] consistent both with theory and previous experiments.[2,3,16,20,21] This standard deviation is negligible compared to the dynamic ranges of features in the OAWRS images and the variations in herring target strength measured across frequency in the OAWRS range.

B. Estimating areal fish population density from instantaneous OAWRS imagery

Here we describe how areal fish population density over wide areas may be estimated from OAWRS intensity images of the ocean environment. At typical OAWRS operating frequencies from hundreds of hertz to a few kilohertz, most fish are acoustically compact scatterers, with swimbladder sizes that are much smaller than the wavelength. The sonar equation approach is then valid for analyzing scattering from fish since the scattered field from each individual is omnidirectional, making propagation and scattering factorable even in a waveguide.[29] The expected scattered intensity from fish aggregations after matched-filtering is dominated by the incoherent intensity or variance of the scattered field and multiple scattering effects are negligible for the densities found here, as shown in Refs. 30 and 31. As a result, given a source at $\boldsymbol{r}_0$ transmitting a broadband signal with bandwidth centered at f_c and a receiver at $\boldsymbol{r}$, the expected scattered intensity, $\langle I_s(\boldsymbol{\rho}_m,f_c)\rangle$, within the OAWRS resolution footprint of area $A(\boldsymbol{\rho}_m|\Delta\rho,f_c)$ centered at horizontal location $\boldsymbol{\rho}_m$ can be expressed as

$$\langle I_s(\boldsymbol{\rho}_m,f_c)\rangle = \sum_{i=1}^{M(\boldsymbol{\rho}_m)} \langle |Q(f_c)|^2\rangle \times (4\pi)^4 \langle |G(\boldsymbol{r}_i|\boldsymbol{r}_0,f_c)G(\boldsymbol{r}|\boldsymbol{r}_i,f_c)|^2\rangle \times \left\langle \frac{|S(\boldsymbol{r}_i,f_c)|^2}{k^2}\right\rangle, \quad (1)$$

where $M(\boldsymbol{\rho}_m)$ is the number of fish within the resolution cell, $\boldsymbol{r}_i$ is the location of the ith fish, $|Q(f_c)|^2$ is the source intensity, $G(\boldsymbol{r}_i|\boldsymbol{r}_0,f_c)$ and $G(\boldsymbol{r}|\boldsymbol{r}_i,f_c)$ are the waveguide Green's functions from the source to each scatterer and from each scatterer to the receiver, respectively, $S(\boldsymbol{r}_i,f_c)$ is the fish scatter function, and k is the wavenumber.

The expected intensity in a fluctuating waveguide from uniformly distributed targets within the resolution footprint can be approximated as

$$\langle I_s(\boldsymbol{\rho}_m,f_c)\rangle \approx \langle |Q(f_c)|^2\rangle \gamma(\boldsymbol{\rho}_m,f_c) \sum_{i=1}^{M(\boldsymbol{\rho}_m)} \left\langle \frac{|S(\boldsymbol{r}_i,f_c)|^2}{k^2}\right\rangle, \quad (2)$$

where $\gamma(\boldsymbol{\rho}_m,f_c)=\langle |(4\pi)^2 G(\boldsymbol{r}_m|\boldsymbol{r}_0,f_c)G(\boldsymbol{r}|\boldsymbol{r}_i,f_c)|^2\rangle$ for sufficiently narrow depth layers H and areal footprints over which $\gamma(\boldsymbol{\rho}_m,f_c)$ becomes effectively constant, as shown for the OAWRS 2006 fish shoal imaging in Ref. 4. The last factor of Eq. (2) can be written as

$$\sum_{i=1}^{M(\boldsymbol{\rho}_m)} \left\langle \frac{|S(\boldsymbol{r}_i,f_c)|^2}{k^2}\right\rangle = \sum_{i=1}^{M(\boldsymbol{\rho}_m)} \int\int\int \frac{|S(\boldsymbol{r}_i,f_c)|^2}{k^2} P(\boldsymbol{r}_i)d\boldsymbol{r}_i^3 = M(\boldsymbol{\rho}_m)\bar{\sigma}(\boldsymbol{\rho}_m,f_c), \quad (3)$$

where $P(\boldsymbol{r}_i)$ is the probability density of finding the ith fish at location $\boldsymbol{r}_i$, and $P(\boldsymbol{r}_i)=1/A(\boldsymbol{\rho}_m|\Delta\rho,f_c)H$ for uniformly distributed fish shoals, $\bar{\sigma}(\boldsymbol{\rho}_m,f_c)$ is the average scattering cross-section of an individual fish over the OAWRS resolution footprint and the depth layer, $n_{A,\mathrm{OAWRS}}(\boldsymbol{\rho}_m)=M(\boldsymbol{\rho}_m)/A(\boldsymbol{\rho}_m|\Delta\rho,f_c)$ is the mean areal fish population density within the resolution footprint, and $A(\boldsymbol{\rho}_m|\Delta\rho,f_c)\approx \rho_m\Delta\rho\beta(\phi,f_c)$ is the range and azimuth-dependent spatial resolution of the OAWRS imaging system.[21]

Inserting Eq. (3) into Eq. (2) and taking $10\log_{10}$ of both sides, we obtain the scattered intensity level in decibels;

$$L(\boldsymbol{\rho}_m,f_c) \approx SL(f_c) + TTL(\boldsymbol{\rho}_m,f_c) + \mathrm{SS}_{\mathrm{OAWRS}}(\boldsymbol{\rho}_m,f_c) + 10\log_{10}(A(\boldsymbol{\rho}_m|\Delta\rho,f_c)), \quad (4)$$

where $L(\boldsymbol{\rho}_m,f_c)=10\log_{10}\langle I_s(\boldsymbol{\rho}_m,f_c)\rangle$, $TTL(\boldsymbol{\rho}_m,f_c)=10\log_{10}\gamma(\boldsymbol{\rho}_m,f_c)$ describes the expected second moment of depth averaged propagation to and from the fish layer averaged over the resolution footprint of the OAWRS system, $SL(f_c)=10\log_{10}\langle |Q(f_c)|^2\rangle$ is the spectral source level, and $\mathrm{SS}_{\mathrm{OAWRS}}(\boldsymbol{\rho}_m,f_c)$ is the scattering strength.

From Eqs. (2)–(4), OAWRS scattering strength can be expressed as

$$\mathrm{SS}_{\mathrm{OAWRS}}(\boldsymbol{\rho}_m,f_c) = \mathrm{TS}_{\mathrm{OAWRS}}(f_c) + 10\log_{10}\langle n_{A,\mathrm{OAWRS}}(\boldsymbol{\rho}_m)\rangle, \quad (5)$$

where $\mathrm{TS}_{\mathrm{OAWRS}}(f_c)=10\log_{10}\bar{\sigma}(\boldsymbol{\rho}_m,f_c)$ in units of dB re 1 m^2 is the target strength corresponding to the average scattering cross-section of an individual fish over the OAWRS resolution footprint and depth layer within the bandwidth centered at f_c.

The terms in Eq. (4) are evaluated separately for each of the four OAWRS LFM waveforms with different center frequencies f_c. A calibrated stochastic transmission loss model based on the parabolic equation[27] for a range-dependent fluctuating ocean waveguide is used to estimate the random Green's functions and determine $TTL(\boldsymbol{\rho}_m,f_c)$ following the approach described in the Appendix E and Ref. 16. Expected source level is estimated from one-way propagated signals received by a desensitized hydrophone on the moving receiver array using the approach of Ref. 16. The two monitoring hydrophones on the source ship were used to verify the source level estimates. Our analysis indicates the source transmitted a stable output over the course of each day.

The application of Eq. (4) to estimate scattering strength from OAWRS imagery is illustrated in Figs. 2 and 3 of Ref. 32 and in Ref. 33. Scattering strength is a useful parameter for characterizing submerged objects, both distant and nearby, because it is independent of the spatially varying transmission loss and areal resolution footprint of the imaging system. Once the target strength expected of an individual fish is known, an areal fish population density image can be obtained from a scattering strength image[33] using Eq. (5). The target strength corresponding to the average scattering cross-section of an individual fish at OAWRS operating frequencies is estimated by matching between OAWRS and CFFS areal fish population density measurements where simultaneous sampling through stationary fish populations is available.

C. Estimates of areal fish population density from CFFS

The CFFS measurements at 38 kHz are used to provide local estimates of areal fish population density.[14,34,35] The 7° 3-dB beamwidth yields an instantaneous circular survey area

TABLE III. Physical parameters of modeled fish species and their measured target strength at 38 kHz with a CFFS.

Species	Atlantic herring	Acadian redfish	Silver hake
L_{FL} (cm)	19–30	15–39	2–35
L_{TL} (cm)	20–34	16–41	2–35
Depth (m)	120–190	120–190	10–75
$\langle TS_{CFFS} \rangle$ (dB)	−39.7[a]	−38.9[b]	N/A
σ_{CFFS} (dB)	1.3[c]	2.4	N/A
ρ_f[d] (kg m^{-3})	1071	1080	1050
ζ[e] (Pa s)	50	50	20
ϵ[f]	5–10	6	8
κ_{nb}[g]	0.05	0.05	0.03
κ_z[h]	x[i]	0.05	0.03

[a]Mean target strength of herring calculated using Eq. (7).
[b]Mean target strength of redfish calculated using equation in Ref. 71.
[c]Standard deviation of derived herring target strength at 38 kHz incorporating fish length and depth distribution from CFFS and trawl surveys.
[d]Fish flesh density.
[e]Viscosity of fish flesh.
[f]major-to-minor-axis ratio of fish swimbladder.
[g]Fish swimbladder volume to fish body volume ratio at neutral buoyancy depth.
[h]Fish swimbladder volume to fish body volume ratio at depth.
[i]x is a linear function of ambient pressure at depth given by $x = \kappa_{nb}(P_{nb}/P_x)$, where P_{nb} is the ambient pressure at neutral buoyancy depth z_{nb}, and P_z is the ambient pressure at any depth z.

of 24 m diameter directly under the survey vessel at 200 m water depth. Volumetric scattering from all targets within the conical beam were measured. The localized areal fish population density in fish m^{-2}, denoted by $n_{A,CFFS}$, can be estimated using

$$n_{A,CFFS} = \frac{4\pi}{\bar{\sigma}_{bs}} \int_{z_1}^{z_2} s_v dz, \tag{6}$$

where s_v is the volume backscattering coefficient[36] in m^{-1}, z_1 and z_2 delimit the depth bounds for fish aggregations, and $\bar{\sigma}_{bs} = 4\pi 10^{\langle TS_{CFFS} \rangle/10}$ is the mean backscattering cross-section of an individual at 38 kHz in units of m^2, where $\langle TS_{CFFS} \rangle$ is the corresponding mean target strength at ultrasonic frequency.

The expected target strength for an individual fish at 38 kHz varies with species, depth, and total fish length. Here, the expected TS_{CFFS} in dB of an individual herring of total length L_{TL} in centimeters at depth z in m is obtained from Eq. (5) of Ref. 37,

$$TS_{CFFS} = 20 \log_{10} L_{TL} - 2.3 \log(1 + z/10) - 65.4, \tag{7}$$

and then converted to σ_{bs}. The mean backscattering cross-section $\bar{\sigma}_{bs}$ is obtained as the weighted average over the total length and depth distribution of the fish aggregations. From trawl surveys of the imaged fish populations in OAWRS, herring was the overwhelmingly dominant species comprising the large shoals, which had small fractions of redfish and silver hake. Estimates of the mean TS_{CFFS} for individual herring and redfish based on our trawl measurements (Appendix A) of the length distribution are provided in Table III. The expected target strength of herring and redfish over similar depth extent at 38 kHz are close, varying at most by 1 dB, albeit their different length distributions. In contrast, their low-frequency target strength near resonance varies significantly, as discussed in Sec. IV C. These modeled TS_{CFFS} values are in good agreement with those obtained by experimentally analyzing the CFFS backscattered field from individual fish distinguishable in the periphery of various aggregations consistent with 0.1 dB mean squared errors reported in Ref. 37.

Figures 4(D) and 4(E) illustrate the application of Eq. (6) to estimate areal fish density for herring aggregations in the 120–180 m water depth range.

D. Estimating low-frequency target strength by matching OAWRS and CFFS population densities

Here we describe our procedure for estimating the low-frequency target strength corresponding to the average scattering cross-section of an individual shoaling herring over the resolution footprint of the OAWRS system by correlating OAWRS data with simultaneous measurements made along CFFS transects. The target strength of herring at 950 and 1125 Hz is found to be significantly higher than at 415 and 735 Hz, making much lower herring densities observable at these higher frequencies. At the lower frequencies of 415 and 735 Hz, the herring target strength is weaker causing the scattered returns to be background saturated at moderate fish densities. Due to the receiving array's sub-aperture design, OAWRS images at 950 Hz have the best cross-range resolution, making this an optimal frequency for wide-area sensing. An alternative approach for target strength estimation, based on differencing pairs of OAWRS wide-area scattering strength images at two distinct frequencies, is applied in Sec. III E to determine target strength at the lower frequencies. The target strength estimates are summarized in Table IV.

Calibrated acoustic targets were deployed on October 2–3 enabling independent and precise geographic charting of OAWRS images. By making small adjustments to the charting speed and array orientation, scattered returns from calibrated targets were accurately charted to the correct range-azimuth resolution cell relative to the source and receiver. This ensures that scattered returns from all other targets, including the fish aggregations, have been accurately charted as well. In this section we focus on data acquired on October 2–3 when calibrated target data were available and present target strength estimates for other days in the Appendix B.

Close to midnight on October 2, both OAWRS and CFFS systems simultaneously co-registered a massive herring shoal between the 150 and 180 m isobaths on the northern flank of Georges Bank, as shown in Figs. 4(A)–4(C). The observations were made continuously over a 90-min period between 23:30 Eastern Daylight Time (EDT) on October 2 and 01:00 EDT on October 3. Measurements from the two systems are highly correlated during the course of the observations because of the statistical stationarity of the fish populations even though their resolution footprints are significantly different. The OAWRS system monitored and sampled the temporal and spatial evolution of the shoal's horizontal morphology at intervals of 75 s without aliasing. Concurrently, the CFFS system crossed the same shoal twice along a U-shaped transect with two parallel transects 1.5 km apart.

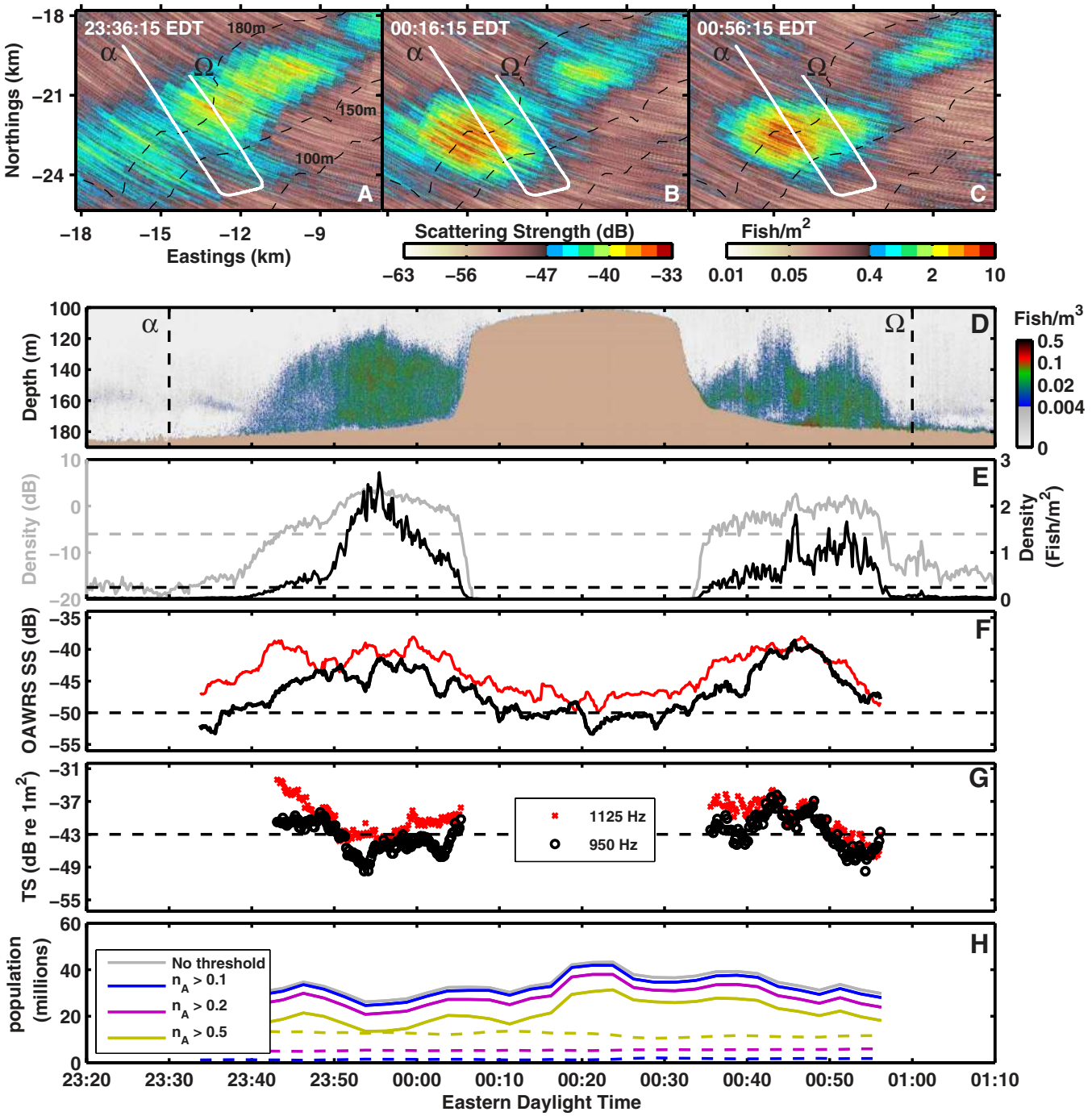

FIG. 4. (Color online) Herring target strength at 950 and 1125 Hz estimated by matching areal fish density in OAWRS and CFFS data acquired during midnight hours of October 2. [(A)–(C)] A sequence of instantaneous OAWRS scattering strength images zoomed into the region containing a massive herring shoal with overlain CFFS line-transect (solid line) made at nominal tow-speed of 2.5 m s^{-1}. (D) CFFS time-depth echogram provides local depth distributions of fish aggregations. Dashed lines at 23:30 EDT and 01:00 EDT correspond to transect start and end points α and Ω, respectively. (E) The areal fish population densities inferred from CFFS measurements following Eq. (6) are plotted as a function of time in black, and the corresponding areal fish population densities in dB, $10\log_{10}(n_{A,\mathrm{CFFS}})$, are plotted in gray. (F) The OAWRS scattering strength measurements and (G) instantaneous target strength estimates along CFFS line-transects at 950 and 1125 Hz. Target strength estimates near the edge of shoals are not accurate because of nonstationarity. (H) Population of herring within the area shown in (A)–(C) determined with various OAWRS fish density n_A thresholds. Solid line gives population above the threshold and dotted line gives population below the threshold.

The depth distribution of the fish population, within roughly 40–60 m of the seafloor, is relatively consistent across the two CFFS transects, as shown in Fig. 4(D).

To accurately estimate low-frequency target strength, we confine our present analysis to contiguous space-time segments that consistently register significant, stationary scattering from fish aggregations in both OAWRS and CFFS systems. We derive threshold values for CFFS population density and OAWRS scattering strength. The segmented data above these thresholds are used for target strength estimation. The CFFS threshold is set at 0.2 fish m^{-2}, as shown in Fig. 4(E). For OAWRS, two square areas of dimension 6.2×3 and 1.57×5.58 km^2 that continuously register significant fish scattering and diffuse background reverberation,

TABLE IV. Mean low-frequency target strength estimates. The $\hat{TS}_{cor}$ estimates are obtained by correlating OAWRS with CFFS data along CFFS transect. This approach is only applied to OAWRS data at 950 and 1125 Hz. For the other frequencies, the $\hat{TS}_{sc}$ estimates are obtained by the approach of differencing OAWRS images. The Diff is the expected target strength difference between the given frequency and 950 Hz.

Date	f_c (Hz)	$\hat{TS}_{cor}$ (dB *re* 1 m^2)	Diff (dB)	$\hat{TS}_{sc}$ (dB *re* 1 m^2)	$\hat{\bar{\sigma}}_{TS}$ (dB)
Oct 2	415	N/A	≈−17.5	≈−60.5	2
	735	N/A	<−8	<−51.0	>3
	950	−43.0	N/A	−43.0[a]	0.7
	1125	−40.3	≈7	≈−36.0	1.7
Oct 3 transect1	415	N/A	≈−17	≈−57.9	2
	735	N/A	≈−8.5	≈−49.4	1.5
	950	−40.9	N/A	−40.9	0.8
	1125	−35.6	≈8	≈−32.9	1.5
Oct 3 transect2	415	N/A	<−17	<−58.7	>3
	735	N/A	≈−7.5	≈−49.2	1.5
	950	−41.7	N/A	−41.7	0.5
	1125	−37.0	≈7.5	≈−34.2	1
Sep 27	415	N/A	<−15	<−57	>3
	735	N/A	≈−12.5	≈−54.5	1.7
	950	−42	N/A	−42	0.7
	1125	N/A	≈5	≈−37	1.5
Sep 29	415	N/A	<−10	<−54.4	>3
	735	N/A	<−7	<−51.4	>3
	950	−44.4	N/A	−44.4	0.8
	1125	N/A	≈10	≈−34.4	2

[a]Base target strength at 950 Hz used in the differencing approach.

respectively, throughout the course of observation are first examined. The histogram of scattering strength values within these areas, averaged over multiple OAWRS images, are plotted in Fig. 5(D). The histograms are approximately Gaussian. The OAWRS threshold is then set at −50 dB for 950 Hz to distinguish fish scattering from the background. This threshold is roughly 2 standard deviations below the mean for the fish histogram and roughly 2 standard deviations above the background mean.

Employing Eq. (5), and assuming local stationarity of fish population, we set the areal fish density within the OAWRS resolution footprint to that simultaneously sampled by CFFS transect through the OAWRS footprint, $n_{A,\mathrm{OAWRS}} \approx n_{A,\mathrm{CFFS}}$. The resulting target strength estimates for fish in these contiguous shoaling regions at 950 Hz are shown in Fig. 4(G). The differences in target strength estimates along the transect are due to the fact that the OAWRS and CFFS systems have different resolution footprint sizes, and so the true mean fish areal densities within the OAWRS resolution cell may be overestimated or underestimated by the CFFS system given nonstationary spatial distributions, as occurred at shoal boundaries. The combination of measurements from many space-time locations from both systems should yield mean target strength estimates with small variance by virtue of the law of large numbers as discussed in Appendix C.

Similar statistical analyses have been conducted for OAWRS data at 1125 Hz, with estimated target strength appearing in Fig. 4(G). This approach is also applied to infer herring target strength at 950 and 1125 Hz using OAWRS and CFFS data on October 3, where two contiguous shoal segments are imaged. Estimated target strengths for these two segments are provided in Table IV. The target strength estimates at 950 Hz for the three data sets are consistent, with a standard deviation of roughly 1 dB.

The approach of this section is not used to estimate target strength at 415 and 735 Hz because the herring are much weaker scatterers at these frequencies, as seen in Fig. 5(A) where only the densest shoal population centers stand above background scattering levels. An alternative approach to estimate herring target strength at these lower frequencies is developed and applied in Sec. III E.

E. Frequency dependence of target strength estimated by differencing OAWRS scattering strength images over wide areas

Here, we develop an alternative approach to estimate target strength expected of an individual shoaling herring by differencing pairs of OAWRS scattering strength images acquired at two distinct frequencies over the entire area of the shoal. We apply this to data at 415 and 735 Hz. The approach is illustrated by the conceptual diagram shown in Fig. 6. From Eq. (5), we observe that scattering strength in areas containing fish increases logarithmically with areal density n_A. Here, f_1 represents a low frequency, such as 415 Hz, where the target strength for fish is lower than at another frequency f_2, such as 950 Hz. The background scattering strength from sources other than fish is expected to be statistically stationary and can be identified by its mean level which is frequency dependent. The total scattering strength measured at any given pixel is a sum of the contribution from fish and other background effects. The difference between the total scattering strength across various pixels at the two frequencies then follows the trend illustrated in Fig. 6(B), where at very low fish densities, the scattering strength is dominated by the background reverberation, and at very high fish densities by fish scattering. The difference in the scattering strength at low fish densities therefore provides a measure of the difference in background reverberation. The difference in the scattering strength at high fish densities is equal to the target strength difference for fish at these frequencies. If the target strength at one of the frequencies is known accurately, then the target strength at the other frequency can be obtained.

This approach is implemented for pairs of OAWRS images using 950 Hz as the base frequency. The difference in scattering strength is calculated and plotted for OAWRS data acquired between 22:00 and 22:45 EDT on October 3 in Figs. 7(A)–7(C) for various frequency pairs. We observe the scattering strength difference in the background is roughly 1 dB between 1125 and 950 Hz, but the fish target strength difference is larger, roughly 7.5 dB. Between 950 and 415 Hz, the background scattering strength difference is roughly 1.5 dB, but the fish target strength difference is more than 17 dB. Between 950 and 735 Hz, no conclusion can be

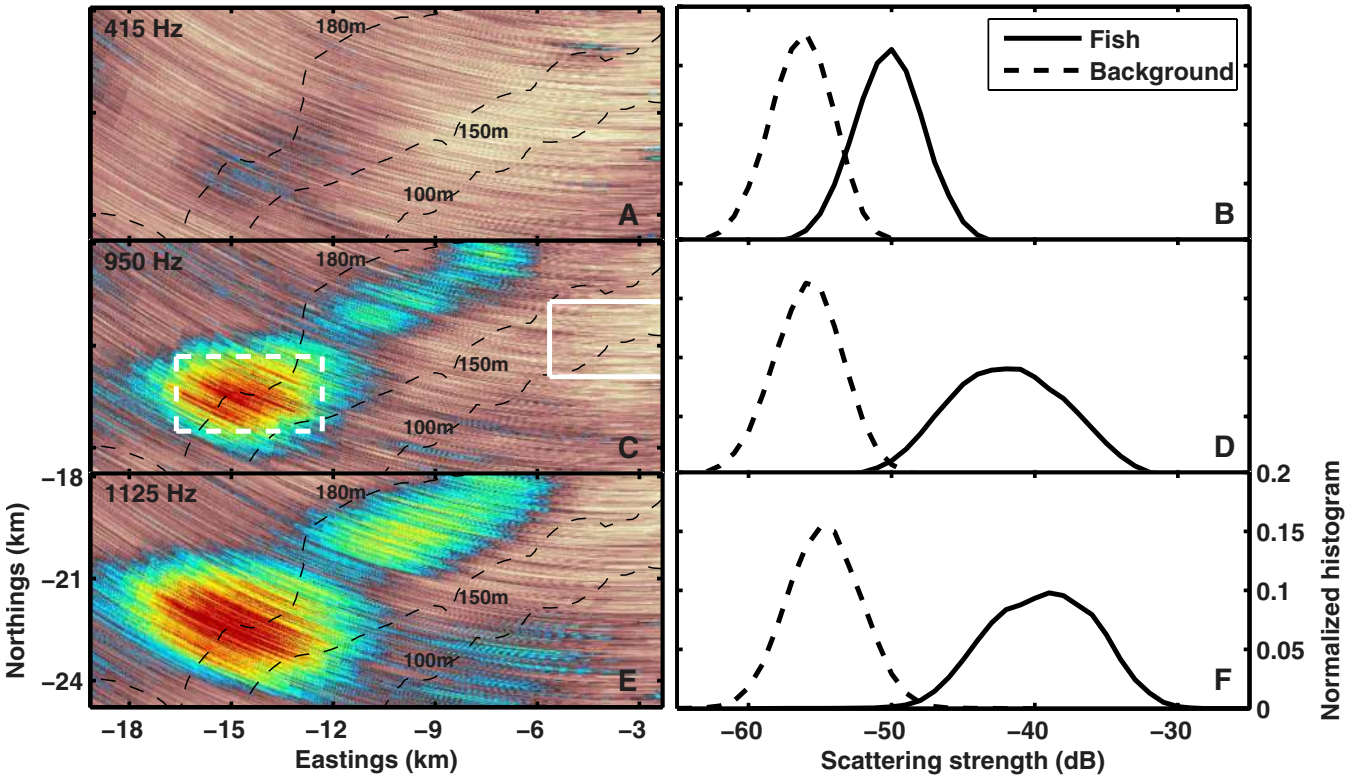

FIG. 5. (Color online) The intensity of scattered returns from shoals is highly frequency-dependent. The histograms illustrate that it is easier to detect shoals over background regions at higher frequencies. Simultaneous trawls show shoals are overwhelmingly comprised of herring while background regions yield negligible herring (Table IV, Fig. 12). [(A), (C), and (E)] OAWRS images of herring shoal acquired simultaneously at three distinct frequency bands centered at 415, 950, and 1125 Hz at 00:41:15 EDT on October 2. The colorscale used in (A), (C), and (E) is the same as in Figs. 4(A)–4(C). [(B), (D), and (F)] Histograms of scattering strength values at locations within the shoal (areas inside the dashed box) and in a background region (areas inside the solid box) plotted for comparison. The 735 Hz data are ambient noise limited in background areas due to weak source level and is not shown.

drawn about background scattering because the 735 Hz data were dominated by ambient and nearby shipping noise since the source level for this frequency was lower. The fish target strength difference between 950 and 735 Hz is roughly 7.5 dB. These results are tabulated in Table IV.

As the OAWRS imaging frequency increases from 415 to 1125 Hz, the target strengths of both fish populations and background levels also increase. From the histograms of Fig. 5, the scattering strength increase with frequency is greater for the fish shoals than background levels, making it easier to detect fish aggregations at the higher frequency. At 415 Hz, only densely populated fish regions are distinguishable from the background. Fish densities at shoal peripheries are typically too low to be detectable.

The background levels in Figs. 7(A)–7(C) can be used to derive the minimum detectable fish densities in the OAWRS system at various frequencies. From Fig. 5(D), if we require that fish returns stand at least 1 standard deviation above the background mean to be detectable, then scattering strength levels that are above roughly −52 dB at 950 Hz would be detectable. This corresponds to a minimum detectable areal density of roughly 0.1 fish m^{-2}. The minimum detectable densities at the other frequencies are tabulated in Table V. These are based on scaling the fish densities up or down depending on the background mean scattering strength level at the other frequencies (Fig. 7) and also accounting for the target strength differences. These results are consistent with those obtained from analyzing the histograms in Fig. 5.

IV. RESULTS AND DISCUSSION

A. Measured abundance

Herring areal population densities and abundances are estimated by subtracting the estimated target strength expected of an individual herring from OAWRS scattering strength images as explained in Sec. III B. Areal fish density is first calculated by applying Eq. (5) at each pixel in an OAWRS image. Integrating over the area of a shoal then provides an estimate of its abundance. We illustrate abundance estimation with OAWRS images generated at 950 Hz since these have the best spatial resolution.

Figures 4(A)–4(C) show the areal fish density for a sequence of instantaneous OAWRS images close to the midnight hours of October 2 where average density within the shoal often exceeds 10 fish m^{-2}. Figure 4(H) shows the population over time within the area shown in Figs. 4(A)–4(C) for consecutive OAWRS images from 23:30 EDT on October 2 to 01:00 EDT on October 3. When no threshold is applied, we simply integrate the densities throughout the area. The total population of roughly 40×10^6 fish includes fish in the shoaling region as well as diffuse fish clouds outside the shoal. Contributions from outside the fish shoal, which may include background from the seafloor, are estimated to account for less than 10% of the total population in the area shown.

To exclude background reverberation, a density threshold is selected to segment shoaling regions where fish scat-

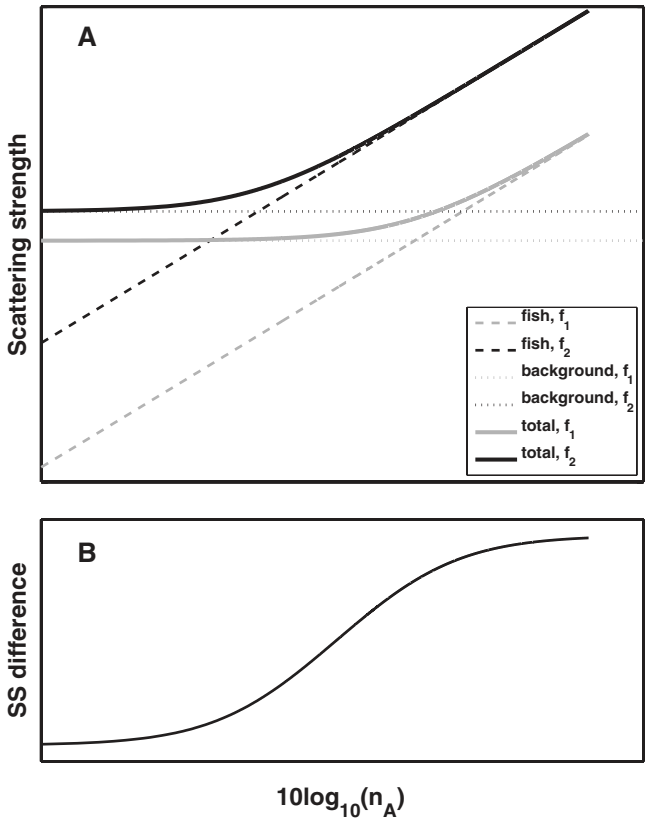

FIG. 6. (A) Schematic of scattering strength levels at two distinct frequencies f_1 and f_2 as a function of local fish density and (B) their difference at a given OAWRS pixel. The scattering strength difference equals the mean background level difference for low fish densities, while at high fish densities, the scattering strength differences equals the fish target strength difference.

tering is dominant. Figure 4(H) shows the total population of fish above and below various density thresholds, 0.1, 0.2, and 0.5 fish m^{-2}. The optimal density threshold for segmenting the shoaling region is roughly 0.2 fish m^{-2} since below this threshold populations stay fairly constant as expected for background levels. This threshold also corresponds to a scattering strength of roughly −50 dB which is roughly the value where the scattering strength histograms for background and shoaling regions intersect in Fig. 5. The population of fish in the shoaling region varies over time between 30×10^6 and 40×10^6.

TABLE V. Minimum detectable fish density (M.D.D) in OAWRS imagery.

f_c (Hz)	415	950	1125
M.D.D (fish m^{-2})	4	0.1	0.04

The massive shoal shown in Fig. 2(A) is comprised of over 240×10^6 fish, with roughly 170×10^6 in the large consolidated shoal and 70×10^6 in the diffuse fish aggregation region. The population of fish in the shoals of Figs. 2(B) and 2(C) are roughly 86×10^6 and 70×10^6, respectively. As discussed in the Appendix D, the uncertainty in the abundance estimate is roughly 17–20%.

B. Measured low-frequency target strength

Following the approach of Secs. III D and III E, the target strength corresponding to the mean scattering cross-section of an individual shoaling herring is estimated as a function of frequency in the 300–1200 Hz range of the OAWRS system from measured scattered returns and measured and modeled transmission loss as shown in Fig. 10 and Table IV. The target strength data show a consistent dependence in both level and roll-off with decreasing frequency of roughly 20 dB/octave for all measurements, which spanned five shoals on 4 days. The invariance of the results from shoal to shoal and day to day is consistent with the low measured standard deviations obtained for each shoal by stationary averaging. The very strong roll-off in frequency is consistent with that found just below the resonance peak of a system undergoing damped harmonic oscillation.[38]

C. Using measured low-frequency target strength to infer swimbladder properties

Air-filled swimbladders typically comprise roughly 5% of fish body volume at neutral buoyancy depth.[39] To remain neutrally buoyant as hydrostatic pressure changes with depth, fish need to regulate the amount of gas in their swimbladders to maintain the 5% ratio.[40] Given this ratio and total

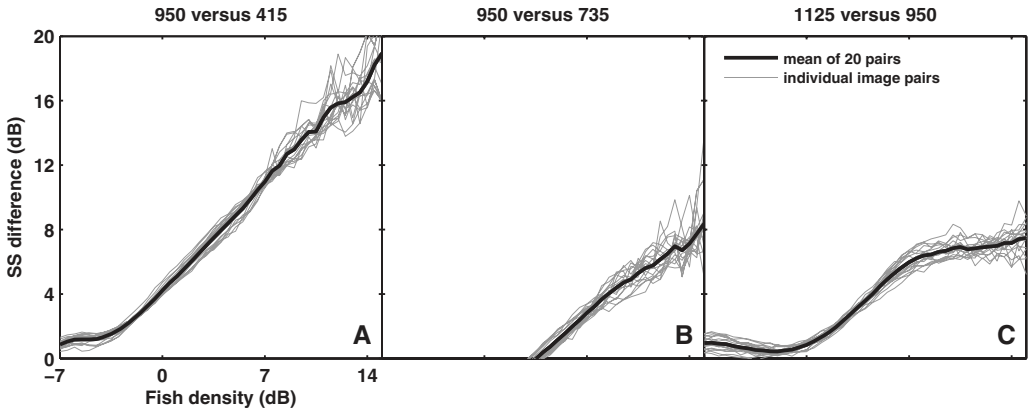

FIG. 7. OAWRS scattering strength level differences for the indicated frequency pairs as a function of areal fish density in dB *re* 1 m^2 for data acquired between 22:00 and 22:45 EDT on October 3. The scattering strength difference at high fish densities equals the target strength difference for the frequency pair shown.

fish volume, swimbladder volume can be determined at any depth as can neutral buoyancy depth if the relationship between pressure and volume is known for the swimbladder. One highly plausible relationship is Boyle's law,[41,42] where the product of pressure and volume remains constant, which has been demonstrated in the laboratory with a single dead herring,[43] but has not been directly confirmed in the wild where it is difficult to make *in situ* measurements of the physiology of free-ranging fish at depth.

Herring are physostomes, fish with open swimbladders connected to the gut and colon.[44] There are three hypotheses by which herring inflate their swimbladders: (1) by gulping air at the surface,[44–47] (2) by bacterial fermentation in the gut,[44,48] and (3) by secretion of gas from the blood stream into the swimbladder.[49–52] Nøttestad[52] found hypotheses (1) and (2) implausible for the Norwegian spring spawing herring in his study that remain in deep layers, are not observed near the surface, and are not feeding. This led him to suggest hypothesis (3). Nero *et al.*[7] conducted on site experiments on the northern flank of Georges Bank with spawning herring by adding weights to captured herring until they sank. They concluded "that these herring contained up to at least a three times greater volume of gas than a neutrally buoyant fish at the sea surface," and arrived at neutral buoyancy depths as great as 60 m from these and low-frequency acoustic target strength measurements. They found their results to be consistent with measurements of Pacific herring in Puget sound,[48] and suggested hypotheses (2) and (3) as plausible explanations for their observations. Similarly, Fänge[51] supported hypothesis (3) by noting that "The herring lacks obvious gas depository structures (*rete mirabile*, gas gland), but has relatively high O_2 values in the swimbladder (up to 21.5%),[53] and observations of release of gas bubbles from vertically migrating herring[54] indicate that some gas secretion may occur."

The conditions of the present experiment were not only similar to those of Nero *et al.*,[7] but also to those of Nøttestad[52] in that the spawning herring were only observed in deep layers and not near the surface where it is unsafe due to predator attack as both Nøttestad[52] and Makris *et al.*[3] noted, and a vast majority of the herring captured in trawl samples were observed to have no large prey (copepods) in their stomachs. The latter point, however, needs to be tempered because bacterial content was indeterminate in the samples, food resources are plentiful near the seafloor where the herring shoals of the present study were found, and gas production by bacteria in herring stomachs can last more than 90 h (Ref. 55) after ingestion. It is typically associated with a delay due to phase lag in bacterial growth.[55] Since the diffusion rate of gas out of the swimbladders of caged herring at fixed depth is also found to be small,[40] corresponding to less than a 0.3 dB decrease in target strength per day, herring may maintain bacterial gas for long periods with minimal feeding on large prey. Such feeding is known to increase with gonadal development.[56] These facts suggest that in addition to Nøttestad's[52] hypothesis (3), hypothesis (2) may also remain highly plausible for our experiment as suggested by Nero *et al.*[7] for a similar location and season.

Here we compare the estimated low-frequency target strength obtained from experimental data with that derived from Love's widely used model for resonant scattering from a fish swimbladder.[6,7,57] This comparison enables estimates of swimbladder volume to be inferred for the shoaling herring observed in this study. Love models the fish swimbladder as an elongated-spheroidal, viscous, heat-conducting shell which encloses an air cavity with surface tension at the inner surface.[6,57] This leads to well-understood damped resonance behavior. While the material in and around the swimbladder has more complex elastic composition and structural constraints than that in the Love model that could lead to more complex scattering, the Love model has been successfully tested in experimental settings where strong resonances have been observed,[6,7,57–61] and probably provides an accurate description of the first order physics near resonance. Following Refs. 7 and 61–64, the swimbladder is modeled as a resonant, air-filled prolate-spheroid with a major-to-minor-axis ratio of 5–10 and major-axis to fish length ratio of 0.13–0.17 based on our trawl samples and CFFS measurements for herring. Only changes in minor-axis are assumed to contribute to swimbladder volume change due to physiological constraints.[7,45,65,66] We use the herring length distribution [Fig. 8(A)] measured from trawl samples and depth distributions determined by CFFS line-transects. The fish weight (W) to length (L) relationship is approximated by a normal distribution with a mean given by an empirically determined length-weight regression (gray line) from length-weight measurement of 1219 herring samples and a standard deviation of $\pm 20\%$ of the mean calculated from the length-weight data (dots), as shown in Fig. 9. Properties of modeled fish, such as the flesh density, viscosity, and swimbladder volume at depth are tabulated in Table III. Given these constraints, swimbladder volume or equivalently swimbladder semi-minor-axis is the only unknown variable in the Love model

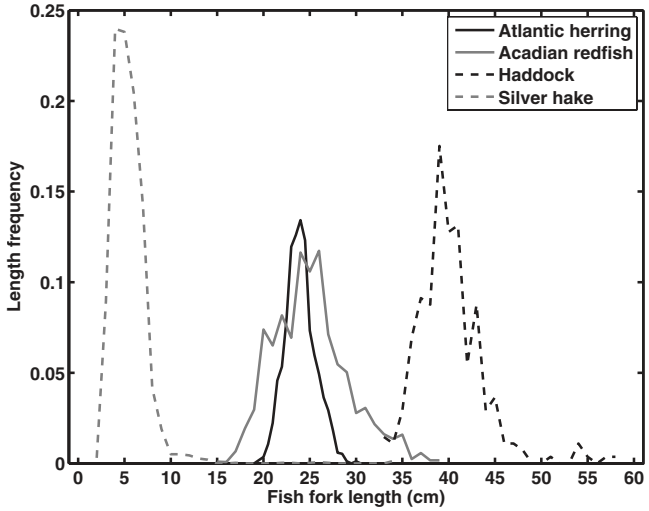

FIG. 8. Fork length distributions of most frequently caught species, Atlantic herring, Acadian redfish, Haddock, and Silver hake, from trawls deployed on Georges Bank (Fig. 1). The mean fork length of herring is 24.2 cm with a standard deviation 6.8% of the 24.2 cm mean. The equation $L_{TL}=1.103L_{FL}+0.01$ (Ref. 7) is used to convert herring's fork length to the total length, where L_{TL} and L_{FL} are in cm. The mean fork length of redfish is 26.2 cm with a standard deviation 15% of the 26.2 cm mean. The equation $L_{TL}=1.033L_{FL}-0.038$ (Ref. 72) is used to convert redfish's fork length to total length. Silver hake's fork length is the total length.

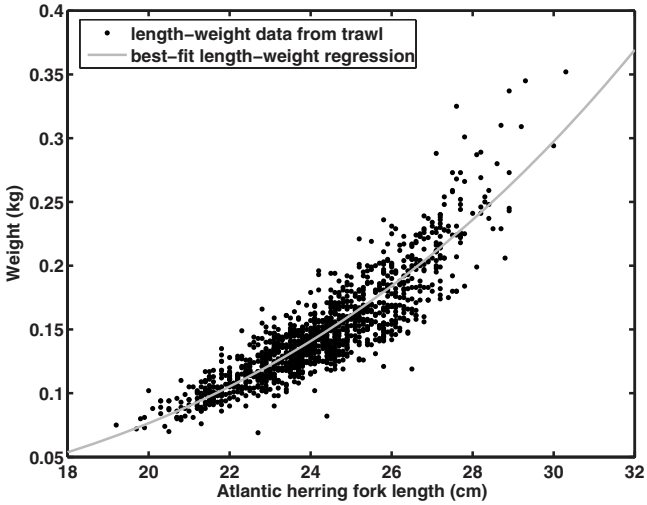

FIG. 9. Atlantic herring length-weight regression calibration. The dots are the length-weight data obtained from the trawl-survey conducted by U.S. National Marine Fisheries Service in conjunction with OAWRS 2006 experiment, and the gray solid line indicates the derived best-fit length-weight regression, which can be expressed as $W=aL^b$, where W is the weight of herring in kg, L is the fork length of herring in cm, and a and b are empirical regression parameters. For this trawl dataset, $a=3.35\times10^{-6}$ and $b=3.35$.

that can lead to a significant change in fish target strength at and below the resonance peak. Swimbladder volume is assumed to vary with pressure according to Boyle's law,[41,42] from which neutral buoyancy depth can be uniquely determined. Neutral buoyancy depth is then assumed to be a Gaussian random variable with mean and standard deviation determined by least-squares fit between measured and modeled target strengths.

The best least square fits between our measured target strength data and the Love model appear in Figs. 10(A)–10(E) for five fish shoals imaged by OAWRS on four different days, and consistently show a broad resonance peak with maximum at roughly 1.5–1.7 kHz and swimbladder semi-minor-axis of 3–5 mm. The model to data match is excellent, with negligible mean-squared error, which is significant because it would not be possible to obtain a good match between the measured frequency dependence and the Love model if the overall level of the measured target strength data had a significant scale factor error that was much larger than measured errors of roughly 1 dB. This consistency gives added confidence to the veracity of both the data and model. As expected from the roughly 20 dB/octave frequency roll-off of the data, the best fit of the model is for a resonance just above the highest frequency data point available in the current set of measurements. The model fits of Fig. 10 can be interpreted with the aid of Table VI which shows the volume and corresponding swimbladder minor axes radii given the measured herring length distributions, as well as possible neutral buoyancy depths based on Boyle's law. Neutral buoyancy depths were found to correspond to roughly half the mean shoal depth given the measured herring length distribution, spanning 20–34 cm with a mean of 26.7 cm, and depth distribution in a layer between 120 and 190 m from trawl and CFFS sampling.

The localized measurements of Nero *et al.*[7] for herring target strength data in the 1.5–5.0 kHz range show target strength levels consistent with those found in our best-fit curve for frequencies above roughly 2.2 kHz. This can be seen by noting their best-fit neutral buoyancy depth curve (50 m) falls within 1–2 dB of ours for all examples above roughly 2.2 kHz for the measured fish depth, length, and density distributions of this study. The Love-model based neutral buoyancy depths and resonances found here are also consistent with those measured by OAWRS in 2003 south of Long Island, NY, in scattering from shoals that evidence suggest were also Atlantic herring.[2,67] Arbitrarily constraining the neutral buoyancy depth to be near the surface, say, at 4 m and using Boyle's law for fish at 120–190 m depth yields a corresponding 3.7 kHz resonance and leads the Love model to a herring target strength 20–30 dB lower (Fig. 11) than that measured by the OAWRS system. Such low target strengths are not only inconsistent with the target strength measurements of Fig. 10 and Nero *et al.*,[7] they also violate conservation of energy since the corresponding transmission losses required to match our measured sound pressure levels returned from the fish shoals would have to be less than those found in even a perfectly reflecting waveguide without any medium attenuation, i.e., the waveguide would have to somehow add energy to the source signal by two to three orders of magnitude. This can be seen in Fig. 14 which shows the measured transmission loss to be within 2–3 dB of that found in a perfectly reflecting waveguide without attenuation.

A wide distribution of swimbladder volumes and corresponding neutral buoyancy depths within any shoal is likely and could potentially unify the various existing data sets by superposition, with larger swimbladder volumes dominating at the lower end of the possible resonance spectrums and smaller volumes dominating the higher end. None of the systems used in the field so far, however, could test this since it would require acquisition of simultaneous data both well below and well above all contributing resonant frequencies. Since low-frequency target strength measurements near resonance are far more sensitive to small changes in swimbladder minor-axis or volume than at much higher CFFS frequencies, such lower frequency measurements have the potential to resolve the *in situ* swimbladder volumes of wild herring at depth with much greater accuracy. The measurements of target strength for herring as a function of depth reported by Ona[37] at 38 kHz, for example, show standard deviations of 8–10 dB and minimal 3–5 dB reduction from the surface to 300 m,[66] which falls well within these standard deviations. These standard deviations significantly exceed the 5.6 dB expected purely from stationary Gaussian field fluctuations by the Central limit theorem,[26] shown to apply to scattering from fish of random orientation by Dahl and Mathisen.[68] This may suggest a bias in fish orientations or a wide spread in swimbladder volumes in the Ona[37] data, which could easily include the span of volumes measured here and in Ref. 7. Fässler *et al.*[43] suggested that projected dorsal area variations exhibit greater depth variation than the mean target strength measurements of Ona.[37] We find the Ona[37] mean trend in depth to be consistent with that expected from Boyle's law since at their frequencies ka, the product of acoustic wavenumber to the semi-minor-axis of the swimbladder, is typi-

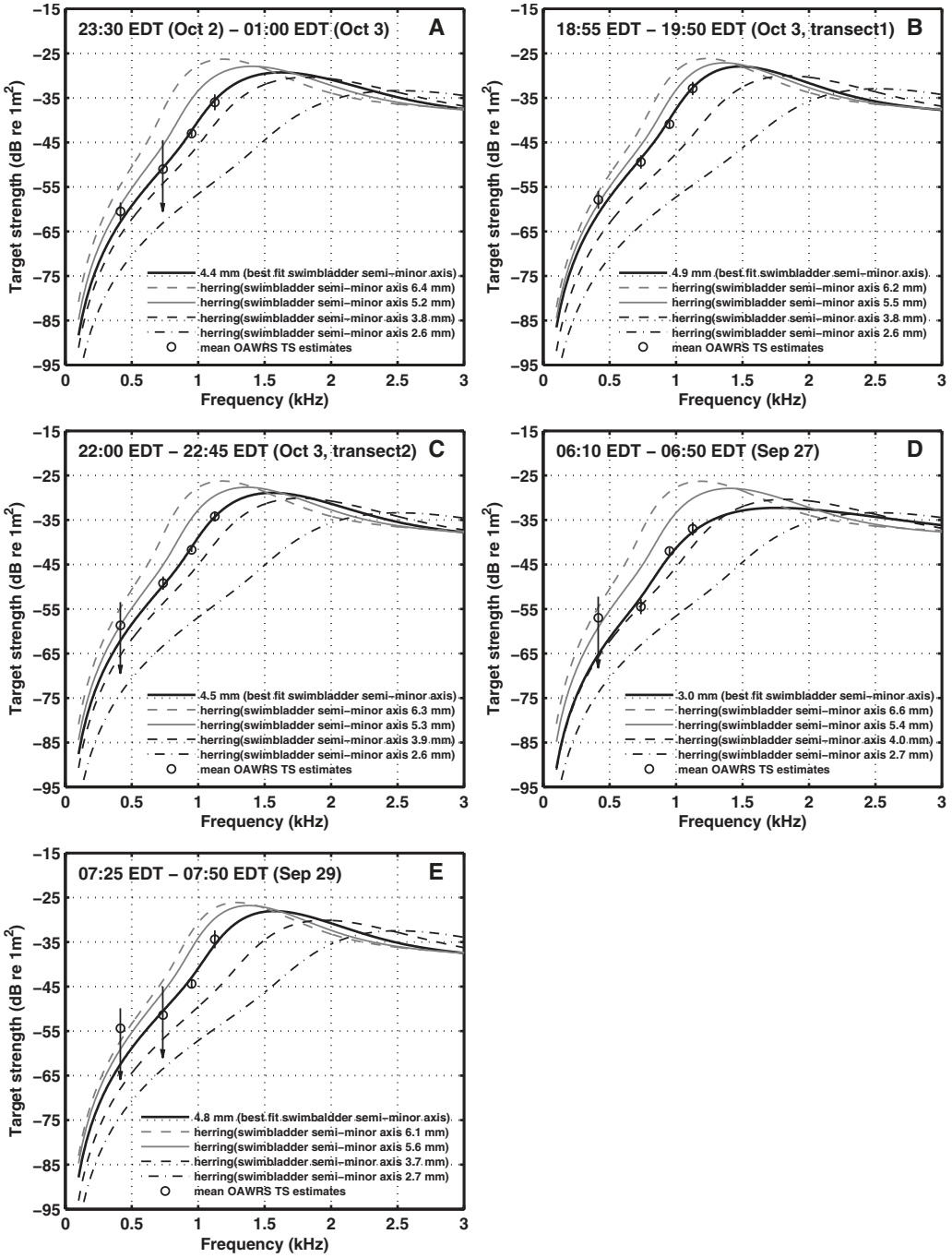

FIG. 10. Experimentally determined low-frequency target strength corresponding to the average scattering cross-sections of shoaling herring observed from OAWRS imagery acquired from five shoals on 4 days (Table VI) at 415, 735, 950, and 1125 (circles) with standard deviations (error bars). Comparison with Love-model mean target strength for shoaling herring, with physical parameters tabulated in Table III, of different swimbladder semi-minor axes over the shoals' depth distributions (lines). The best least-squares fits shown are obtained only using target strength estimates of each shoal (Table IV) with standard deviations less than 3 dB. Arrows indicate the target strength uncertainties due to potential masking from background scattering (Sec. III E) for given frequencies. The best-fit means and standard deviations of inferred swimbladder volume, swimbladder semi-minor axes, and corresponding neutral buoyancy depths of each shoal were tabulated in Table VI. (A) Shoaling herring, distributed between 120 and 185 m (Fig. 4), imaged with the OAWRS system from 23:30 EDT October 2 to 01:00 EDT on October 3. (B) Shoaling herring, distributed between 135 and 175 m, imaged with the OAWRS system from 18:55 to 19:50 EDT on October 3. (C) Shoaling herring, distributed between 120 and 175 m, imaged with the OAWRS system from 22:00 to 22:45 EDT on October 3. (D) Shoaling herring, distributed between 120 and 185 m, imaged with the OAWRS system from 06:10 to 06:50 EDT on September 27 (Fig. 13). (E) Shoaling herring, distributed between 150 and 180 m, imaged with the OAWRS system from 07:25 to 07:50 EDT on September 29.

cally less than unity and target strength is no longer proportional to projected area as in the large *ka* limit.

Evidence from the extensive OAWRS, CFFS, and trawl surveys conducted during OAWRS 2006 offers no plausible alternative to herring as the primary constituent and source of scattering in the shoals imaged by OAWRS. Consideration of the effect of two other species, however, also present in many trawls but in far fewer numbers (Table VII), still provides useful perspective. These are silver hake and Acadian redfish. While silver hake were found at shallower depths than herring, their much shorter lengths (Fig. 8) lead to individual target strengths more than 20 dB lower than those

TABLE VI. Experimentally inferred means and standard deviations of swimbladder volume, $\hat{v_{sb}}$ and $\sigma_{v_{sb}}$, semi-minor-axis, $\hat{a_z}$ and σ_{a_z}, over the depth distributions of the shoals, and corresponding means and standard deviations of neutral buoyancy depth, $\hat{d_{nb}}$ and $\sigma_{d_{nb}}$, where neutral buoyancy depth is restricted to water-column depths of 0–200 m in the least squares fit. All three parameters are assumed to be Gaussian random variables completely characterized by their respective means and standard deviations.

Date	Time[a]	Layer depth (m)	$\hat{v_{sb}}$ (ml)	$\sigma_{v_{sb}}$ (ml)	$\hat{a_z}$ (mm)	σ_{a_z} (mm)	$\hat{d_{nb}}$ (m)	$\sigma_{d_{nb}}$ (m)
Oct 2	23:30–01:00(Oct 3)	120–185	3.41	0.41	4.4	0.26	82	11
Oct 3	18:55–19:50	135–175	4.27	0.31	4.9	0.18	108	9
Oct 3	22:00–22:45	120–175	3.62	0.38	4.5	0.24	85	10
Sep 27	06:10–06:50	120–185	1.61	1.49	3.0	0.96	31	48
Sep 29	07:25–07:50	150–180	3.98	0.21	4.8	0.12	107	6

[a]Time periods during which both OAWRS and CFFS systems simultaneously co-registered contiguous shoal segments. The time is in EDT.

measured at the location of the herring shoals at OAWRS frequencies (Fig. 11). Given that (1) both CFFS and trawl samples found silver hake in considerably lower areal densities than herring, (2) their individual target strengths are roughly 20 dB lower, and (3) OAWRS transmission loss was much greater in the shallower layers where silver hake resided as part of the experimental design, contributions from silver hake can be ruled out as a plausible explanation for shoals imaged by OAWRS. As shown in Fig. 11(A), the presence of redfish in the maximum percentages determined by trawl has a negligible effect on the best-fit target strength compared to that of modeling herring alone [Figs. 10(A)–10(E)]. This should be expected because the low-frequency dependence of background returns when no shoals are present is effectively negligible compared to the dependence when shoals are present (Fig. 5) and simultaneous trawls showed the shoals to be overwhelmingly comprised of herring but the background to yield negligible amounts of herring (Table IV, Fig. 12). So, even though redfish are physoclists with trawl sample lengths (Fig. 8) typically greater than those of the herring, the measured areal densities of redfish are too low to have a significant impact on the average scattering cross-section measured in the observed shoals. Including greater percentages of redfish in the modeling or including measured percentages and shallower neutral buoyancy depths for herring leads to far worse fits and high mean-square error when matched with the data, as shown in Fig. 11(B).

D. Space, time, and frequency dependencies

From another perspective, since the spatio-temporal population distributions of the large shoals versus background levels are consistent among OAWRS, CFFS, and trawls, as shown here and in Ref. 3, the spatio-temporal distributions of silver hake, redfish, or any other contaminant

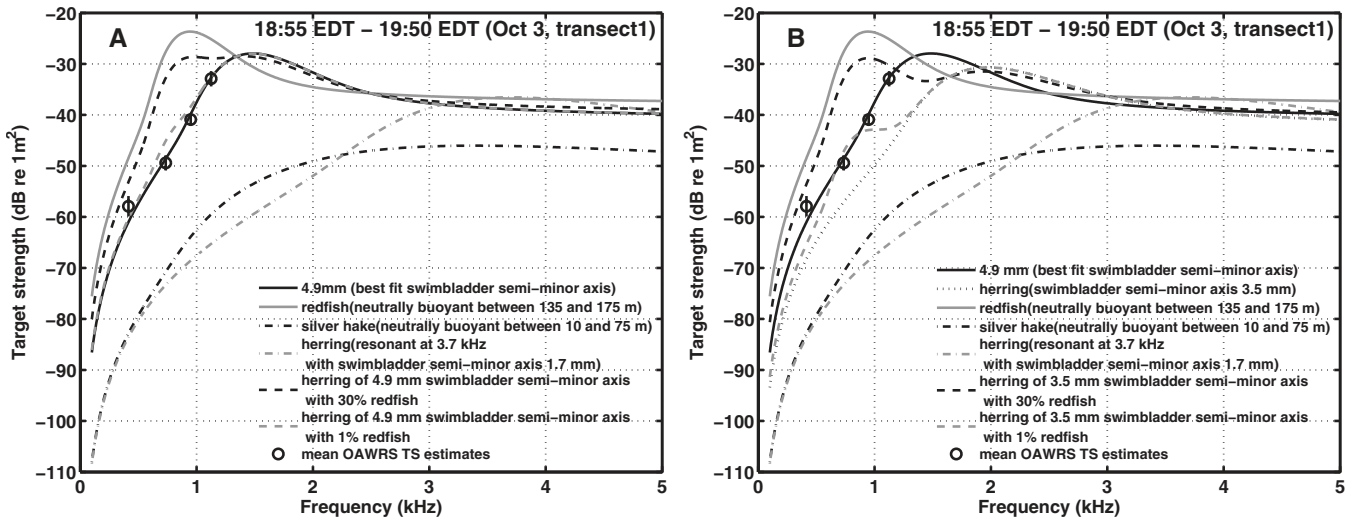

FIG. 11. (A) An example of Love-model target strength corresponding to the average scattering cross-section of an individual for mixed species content and swimbladder semi-minor axes shown. Comparison of Love-model target strength with experimentally determined mean target strength estimates of shoaling herring, distributed between 135 and 175 m, imaged with the OAWRS system from 18:55 to 19:50 EDT on October 3. Presence of redfish in trawl-determined percentage (dashed gray line) has negligible effect on best-fit target strength compared to herring alone (solid black line), while including an unrealistic percentage of redfish yields far worse fits (dashed black line). The silver hake, found at shallower water depth (<75 m) in trawls, have resonance peak above 3 kHz (dash-dot curve) making their contribution negligible. Herring target strength with a resonance frequency at 3.7 kHz (dashed gray line) based on Love's model using length and depth distribution obtained from CFFS and trawl measurements is found to be neutrally buoyant at 4 m, and is 20–30 dB lower than those measured by the OAWRS system. (B) Same as (A) but for shallower herring neutral buoyancy depths. Arrows indicate potential target strength uncertainties for given frequencies.

TABLE VII. Concurrent high-speed rope trawl deployed by NOAA FRV *Delaware II* within or in the vicinity of large herring shoals imaged by OAWRS during the OAWRS 2006 experiment in the Gulf of Maine and Georges Bank at shoal depth. The number of most frequently caught species in each trawl deployment, including Atlantic herring, Acadian redfish, Silver hake, and Haddock are tabulated. Trawls 134, 137, and 139 were made with simultaneous OAWRS imagery, and trawls 137 and 139 were made directly through shoals as shown in Figs. 12(B) and 12(C). In contrast, trawl 134 was made in a region with no shoal formed (Fig. 12(A)), but one shoal would form in the vicinity 4 h later. Trawl 105 was made through shoals imaged by OAWRS 95 min before, and trawl 106 was made through shoals imaged by OAWRS 20 min later.

Deployment	Atlantic herring	Acadian redfish	Silver hake	Haddock	Total catch
105	8030 (99.98%)	0	0	0	8032
106	634 (96.79%)	0	14 (2.14%)	2 (0.31%)	655
134	3 (11.54%)	0	14 (53.85%)	0	26
137	333 (76.03)	0	94 (21.46%)	0	438
139	796 (74.74%)	9 (0.85%)	208 (19.53%)	23 (2.16%)	1065
Total catch of experiment	9796 (96.54%)	9 (0.07%)	330 (2.67%)	25 (0.2%)	10216

species would have to consistently follow those of herring if they were a major contributor to OAWRS returns, which is both implausible and contrary to trawl and CFFS data as well as the frequency dependence of OAWRS returns in shoals versus background (Fig. 5). Also, neither our trawl nor CFFS data show any evidence of shallow fish layers that could account for the prominent OAWRS returns that co-registered in space and time with the deep shoals measured by simultaneous trawl and CFFS sampling. Indeed, considering experimental causality, it was consistently necessary for OAWRS to *first find* and *then direct* trawl and CFFS vessels to the locations of these deep shoals because they are so difficult to find with conventional methods given the fact they occupy areas many orders of magnitude smaller than the wide areas over which they may roam.

V. CONCLUSION

The low-frequency target strength of Atlantic herring (*Clupea harengus*) is estimated from experimental data acquired from shoaling herring in the Gulf of Maine during the Autumn 2006 spawning season in the 300–1200 Hz range using simultaneous ocean acoustic waveguide remote sensing, conventional fish finding sonar, and trawl surveys. The target strength expected of an individual is found to have a strong nonlinear dependence on frequency consistent with resonant scattering from an air-filled swimbladder given measured fish length, depth distributions, and experimentally inferred swimbladder volumes based on Love's model, which indicate the herring remain negatively buoyant in layers near the seafloor for extended periods. The OAWRS system used in this study employed an instantaneous imaging diameter of 100 km with regular minute-to-minute updates enabling unaliased monitoring of fish populations over ecosystem scales. This included detection and imaging of shoals of Atlantic herring containing hundreds of millions of individuals, as confirmed by concurrent trawl and CFFS surveys that were directed to the shoals' locations by OAWRS. High spatial-temporal coregistration was found between herring shoals imaged by OAWRS and concurrent CFFS line-transects.

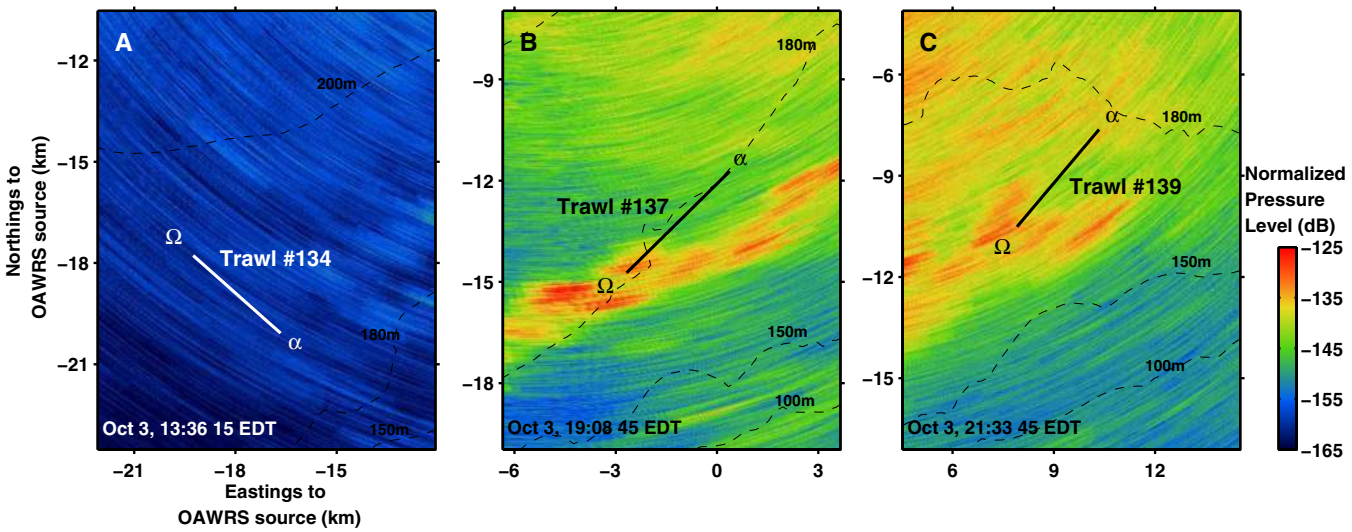

FIG. 12. (Color online) [(A)–(C)] Locations of trawls over simultaneous OAWRS images. Trawls 137 and 139 were made directly through shoals as shown in (B) and (C). In contrast, trawl 134 was made in a region with no shoal (A), but one shoal would form in the vicinity 4 h later. The OAWRS source locations are the coordinate origin in all OAWRS images. On October 3, the OAWRS source ship was moored at 42.2089N, 67.6892W. The trawls in (A)–(C) were deployed and towed along the solid lines starting at α and ending at Ω. The dashed lines indicate the contours of 100, 150, 180, and 200 m water depth.

TABLE VIII. Concurrent high-speed rope trawl deployed by NOAA ship FRV *Delaware II* within or in the vicinity of large herring shoals imaged by OAWRS system during the OAWRS 2006 experiment in the Gulf of Maine and Georges Bank at shoal depth. The dates, times (Eastern Daylight Time), deploy depths, and geographic locations of the trawls are tabulated.

Deployment	Date	Time	Deploy depth (m)	Begin Lat	Begin Lon	End Lat	End Lon
105	09/26	14:21:40-15:16:32	130–160	41° 53.00N	68° 06.62W	41° 51.95N	68° 10.45W
106	09/26	19:23:24-19:57:20	130–160	41° 55.49N	68° 03.80W	41° 55.05N	68° 06.33W
134	10/03	13:21:12-13:54:01	140–170	42° 01.80N	67° 53.39W	42° 03.06N	67° 55.24W
137	10/03	18:47:09-19:27:04	140–170	42° 06.36N	67° 41.02W	42° 04.76N	67° 43.27W
139	10/03	21:16:35-21:52:46	140–170	42° 08.54N	67° 33.83W	42° 07.00N	67° 35.63W

ACKNOWLEDGMENTS

This research was supported by the National Oceanographic Partnership Program, the Office of Naval Research, the Alfred P. Sloan Foundation, and the National Oceanic and Atmospheric Administration and is a contribution to the Census of Marine Life. We would like to thank the science parties, officers, and crew of the research vessels *Oceanus, Endeavor, Delaware II*, and *Hugh Sharp*. We would also like to thank Olav Rune Godø and Redwood W. Nero for the many interesting discussions on the topic, and the research assistants who helped in the data analysis.

APPENDIX A: CONCURRENT NATIONAL MARINE FISHERIES SERVICE ANNUAL ATLANTIC HERRING ACOUSTIC SURVEY IN THE GULF OF MAINE

In conjunction with OAWRS 2006 experiment, U.S. National Marine Fisheries Service conducted annual Atlantic herring survey of the Gulf of Maine and Georges Bank. Five trawls, 105, 106, 134, 137, and 139, targeted at 130–170 m depth (Table VIII) were deployed within or in the vicinity of the large fish shoals imaged by OAWRS system, which enabled onsite species identification and biological measurements. The locations of these trawls are shown in Fig. 1. The trawls 134, 137, and 139 were made with simultaneous OAWRS imagery, and trawls 137 and 139 were made directly through shoals, as shown in Figs. 12(B) and 12(C). As tabulated in Table VII, Atlantic herring is found consistently to be the overwhelmingly predominant species in trawls 105, 106, 137, and 139. Trawl 134, shown in Fig. 12(A), was deployed in a region with no shoal formed, but one would form in the vicinity 4 h later, and like both OAWRS and CFFS does not show high concentrations of herring before the shoal formed. Trawl 105 was made through shoals imaged by OAWRS 95 min before, and trawl 106 was made through shoals imaged by OAWRS 20 min later. In addition, a small percentage of juvenile silver hake, Acadian redfish, and haddock are also present in the trawls. Most of the juvenile silver hake were caught at shallower water depth (<75 m) as the deeper trawls were deployed. Histograms of the measured length distributions of the most frequently caught species are plotted in Fig. 8. The conversion of herring length to weight by regression analysis is given by $W=0.003\,35L^{3.35}$, based on length-weight measurements of 1219 herring caught in trawls throughout the course of the survey.

APPENDIX B: ESTIMATING LOW-FREQUENCY TARGET STRENGTH OF SHOALING HERRING WITHOUT CALIBRATED TARGET DEPLOYMENT

Here we present the estimated low-frequency target strength of a shoaling herring based on simultaneous OAWRS and CFFS sampling line-transects of large shoals on September 27 and 29, 2006 when no calibrated targets were available to aid in charting. Only minor adjustments of less than 1.5° from the array heading sensors were needed to ensure optimal coregistration between OAWRS and CFFS locations of shoals, which were typically the only landmark available in the absence of the calibrated targets. The target strength estimates shown here are consistent with those presented for the other days when calibrated targets were available in the main text.

During the early morning hours of September 27, between 06:10 and 06:50 EDT, both OAWRS and CFFS coregistered a massive herring shoal 10–15 km southeast of the OAWRS source, spanning more than 2 km in range and 5 km in azimuth, as shown in Figs. 13(A)–13(C). A dense layer of herring, shown in Fig. 13(D), was found consistently spanning 120–170 m in the water column by simultaneous CFFS line-transects. The resulting target strength estimates at 950 Hz obtained by means of the approach described in Sec. III D are plotted in Fig. 13(G). The target strength estimates at 415, 735, and 1125 Hz are tabulated in Table IV using the approach described in Sec. III E, where target strength at 950 Hz is used as the base frequency. No conclusion can be made for the target strength difference between 950 and 415 Hz, because fish density is not high enough to make scattering from herring at 415 Hz distinguishable from background levels. The same approaches are also applied to estimate the target strength expected for an individual shoaling herring imaged on September 29 between 07:25 and 07:50 EDT. The results are provided in Table IV.

APPENDIX C: STATISTICAL ANALYSIS FOR LOW-FREQUENCY TARGET STRENGTH OF HERRING

Here we describe the statistical approach used to estimate the mean and standard deviation of the low-frequency target strength of fish populations imaged concurrently by OAWRS and CFFS. We confine our analysis to regions where both systems image continuous segments of statisti-

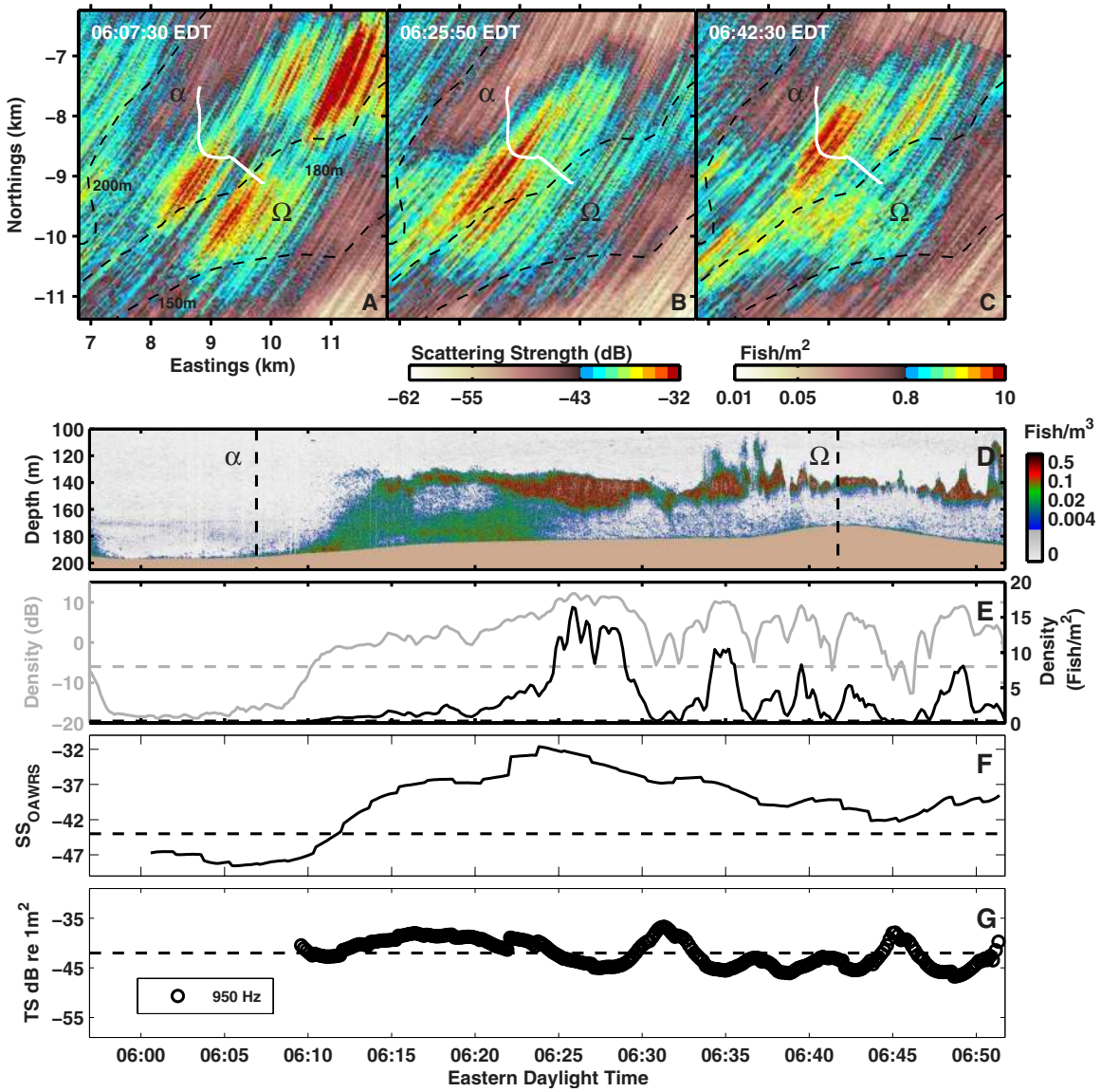

FIG. 13. (Color online) Herring target strength at 950 Hz estimated by matching the areal density of OAWRS and CFFS data acquired during the early morning hours of September 27. Similar to Fig. 4 but for a contiguous shoal 40-min segment starting at 06:10 EDT on September 27.

cally stationary fish populations that span many resolution cells in both the CFFS and OAWRS systems.

Employing Eq. (5), let TS_i be independent estimates of low-frequency target strength obtained for each resolution cell after sufficient spatial and temporal averaging in anti-log to eliminate the bias when converted to log units and to insure that the TS_i are Gaussian random variables.[26] Assuming stationarity, let their means be $\overline{TS}$ and standard deviations be σ_{TS}. Then, given N independent measurements of the target strength along the CFFS transect, the resulting linear estimator for mean target strength is[69]

$$\widehat{\overline{TS}} = \frac{1}{N}\sum_{i=1}^{N} TS_i \tag{C1}$$

and the corresponding estimator for the standard deviation of the target strength distribution is obtained by[69]

$$\hat{\sigma}_{TS} = \sqrt{\frac{1}{(N-1)}\sum_{i=1}^{N}(TS_i - \widehat{\overline{TS}})^2}. \tag{C2}$$

The variance of the mean target strength estimate is

$$\mathrm{Var}(\widehat{\overline{TS}}) = \frac{\hat{\sigma}_{TS}^2}{N}. \tag{C3}$$

Applying Eq. (C3), the standard deviation in the mean target strength estimate for the data in Fig. 4 is roughly on the order of 0.7–0.8 dB.

APPENDIX D: QUANTIFYING ERROR IN ABUNDANCE ESTIMATES

Here we quantify the error in the abundance estimates from OAWRS data presented in this paper. From Eqs. (4) and (5), error in $n_{A,\mathrm{OAWRS}}$ at any pixel is caused by a fixed OAWRS target strength estimate, which is the same for all

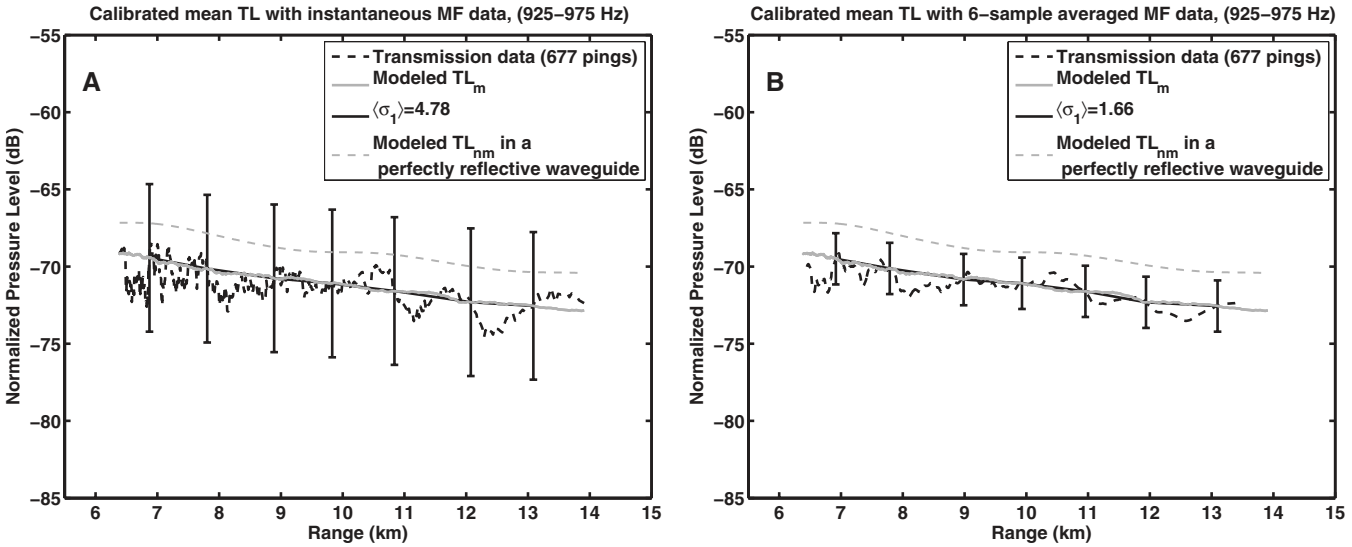

FIG. 14. (A) Experimentally determined mean and standard deviation (4.78 dB) of 677 measured instantaneous broadband one-way TL data after matched filter with 950 Hz center frequency. Plotted as a function of range, with modeled one-way TL overlain. Transmission data acquired by a single desensitized hydrophone on OAWRS receiver array on October 1–3 2006. Modeled TL computed by Monte-Carlo simulation with parabolic equation inputing measured oceanography and bathymetry of Georges Bank environment. Modeled TL (dashed gray line) in a perfectly reflective waveguide with no water-column attenuation by normal-mode model. (B) After six-sample averaging, the rms error is reduced to 1.7 dB, consistent with theory for stationary averaging of intensities of circular complex Gaussian random fields (Refs. 16 and 26).

pixels, and the OAWRS scattering strength, which varies from pixel to pixel. Summing large numbers of pixels reduces the percentage error from scattering strength fluctuations in the population density estimate to negligible values by the law of large numbers, leaving the error to be dominated by that in the OAWRS target strength estimate, which for the 950 Hz imagery is consistently between 0.7 and 0.8 dB throughout the experiment, corresponding to an error of 17–20% in total population.

APPENDIX E: CALIBRATION OF BROADBAND MEAN TL WITH ONE-WAY PROPAGATED EXPERIMENTAL DATA IN THE NORTHERN FLANK OF GEORGES BANK

In wide-area sonar applications, two-way TL must be efficiently and accurately estimated in order to invert for scattering strength or target strength of scatterers.[2,32] Here, RAM is used to estimate two-way TL expected over wide areas with measured bathymetry and oceanography of the northern flank of Georges Bank environment. For each OAWRS image, TL was computed along radials separated by roughly 1.5°, half the receiver array broadside resolution, for forward transmission from the source, and again for return transmission to the receiver array, by multiple Monte-Carlo realizations per radial. Each Monte-Carlo realization employed a different measured sound speed profile every 500 m to incorporate the effects of the fluctuating ocean waveguide.

In the OAWRS 2006 experiment, a very complete set of more than 12 000 transmission loss measurements spanning ranges from hundreds of meters to tens of kilometers, and more than roughly 200 sound speed profile measurements were made over the survey area. These were used to calibrate the parabolic equation model used to estimate wide-area transmission loss, population density, and target strength. Measured sound speed was found to follow a roughly Gaussian distribution about the mean at each depth and to be relatively uniform in time and space over the entire OAWRS imaging area (Fig. 3) with no evidence of horizontal features besides the expected short term fluctuations from internal wave activity.

The best fit between measured and modeled transmission loss was obtained for expected sandy bottom conditions of sound speed of 1.7 km s^{-1}, density of 1.9 g cm^{-3} and attenuation of 0.8 dB λ^{-1}, and in-water-column attenuation of 6×10^{-5} dB λ^{-1}, as shown in Fig. 14 using the maximum likelihood method.[16] Figure 14 shows the standard deviation of one-way TL for instantaneous broadband measurements is roughly 4.8 dB, and after six-sample averaging is on the order of 1.7 dB, following previous experimental results and theory.[16,26] We find the mean measured TL to be within 2–3 dB of that of a perfectly reflecting lossless waveguide of the same depth (dashed gray line in Fig. 14). The *scattered field from large fish shoals* after *two-way propagation in a waveguide* also obeys circular complex Gaussian field statistics by the central limit theorem and has experimentally measured standard deviation of roughly 1.5 dB, after our standard six-sample averaging, for the current experiment[4] which also follows that expected from theory and numerous past experiments where internal waves, ocean turbulence, eddies, and variations in scatterer orientation have been shown to cause short term intensity fluctuations with a standard deviation that can be reduced to a small fraction of the mean after stationary averaging.[20,21,24,26,67,70]

[1]http://www.gma.org/herring/ (Last viewed January 29, 2009).
[2]N. C. Makris, P. Ratilal, D. T. Symonds, S. Jagannathan, S. Lee, and R. W. Nero, "Fish population and behavior revealed by instantaneous continental shelf-scale imaging," Science **311**, 660–663 (2006).
[3]N. C. Makris, P. Ratilal, S. Jagannathan, Z. Gong, M. Andrews, I. Bertsa-

tos, O. R. Gødo, R. W. Nero, and J. M. Jech, "Critical population density triggers rapid formation of vast oceanic fish shoals," Science **323**, 1734–1737 (2009).
[4]N. C. Makris, P. Ratilal, S. Jagannathan, Z. Gong, M. Andrews, I. Bertsatos, O. R. Godø, R. W. Nero, and J. M. Jech, "Critical population density triggers rapid formation of vast oceanic fish shoals," materials and methods are available as supporting material on *Science* online (2009).
[5]B. S. McCartney and A. R. Stubbs, "Measurement of the acoustic target strength of fish in dorsal aspect, including swimbladder resonance," J. Sound Vib. **15**, 397–420 (1971).
[6]R. H. Love, "A comparison of volume scattering strength data with model calculations based on quasisynoptically collected fishery data," J. Acoust. Soc. Am. **94**, 2255–2268 (1993).
[7]R. W. Nero, C. H. Thompson, and J. M. Jech, "*In situ* acoustic estimates of the swimbladder volume of Atlantic herring (*Clupea harengus*)," ICES J. Mar. Sci. **61**, 323–337 (2004).
[8]K. G. Foote, "Importance of the swimbladder in acoustic scattering by fish: A comparison of gadoid and mackerel target strengths," J. Acoust. Soc. Am. **67**, 2084–2089 (1980).
[9]D. V. Holliday, "Resonance structure in echoes from schooled pelagic fish," J. Acoust. Soc. Am. **51**, 1322–1332 (1972).
[10]R. W. Nero, C. H. Thompson, C. Feuillade, and R. H. Love, "A highly reflective low cost backscattering target," IEEE J. Ocean. Eng. **26**, 259–265 (2001).
[11]T. K. Stanton, D. Chu, J. M. Jech, and J. D. Irish, "A broadband echosounder for resonance classification of swimbladder-bearing fish," in Proceedings of the 2007 IEEE Oceans Conference, Aberdeen, Scotland, (2007).
[12]W. J. Overholtz, "The Gulf of Maine-Georges Bank Atlantic herring (*Clupea harengus*): Spatial pattern analysis of the collapse and recovery of a large marine fish complex," Fish. Res. **57**, 237–254 (2002).
[13]W. J. Overholtz and K. D. Friedland, "Recovery of the Gulf of Maine herring (*Clupea harengus*) complex: perspectives based on bottom trawl survey data," Fish. Bull. **100**, 593–608 (2002).
[14]W. J. Overholtz, J. M. Jech, W. L. Michaels, L. D. Jacobson, and P. J. Sullivan, "Empirical comparisons of survey design in acoustic surveys of Gulf of Maine-Georges Bank Atlantic herring," J. Northw. Atl. Fish. Sci. **36**, 127–144 (2006).
[15]N. C. Makris and P. Ratilal, "OAWRS Gulf of Maine 2006 Experiment Cruise Report," sponsored by the Office of Naval Research and Alfred P. Sloan Foundation, 19 September–6 October, 2006.
[16]M. Andrews, T. Chen, and P. Ratilal, "Empirical dependence of acoustic transmission scintillation statistics on bandwidth, frequency, and range on New Jersey continental shelf," J. Acoust. Soc. Am. **125**, 111–124 (2009).
[17]C. I. Malme, "Development of a high target strength passive acoustic reflector low-frequency sonar applications," IEEE J. Ocean. Eng. **19**, 438–448 (1994).
[18]E. T. Küsel and P. Ratilal, "Effects of incident field refraction on scattered field from vertically extended cylindrical targets in range-dependent ocean waveguides," J. Acoust. Soc. Am. **125**, 1930–1936 (2009).
[19]N. C. Makris and J. M. Berkson, "Long-range backscatter from the Mid-Atlantic Ridge," J. Acoust. Soc. Am. **95**, 1865-1881 (1994).
[20]N. C. Makris, L. Z. Avelino, and R. Menis, "Deterministic reverberation from ocean ridges," J. Acoust. Soc. Am. **97**, 3547–3574 (1995).
[21]P. Ratilal, Y. Lai, D. Symonds, L. A. Ruhlmann, J. R. Preston, E. K. Scheer, M. T. Garr, C. W. Holland, J. A. Goff, and N. C. Makris, "Long range acoustic imaging of the continental shelf environment: The Acoustic Clutter Reconnaissance Experiment 2001," J. Acoust. Soc. Am. **117**, 1977–1998 (2005).
[22]T. C. Weber, H. Pena, and J. M. Jech, "Multibeam and single-beam sonar observations of Atlantic herring in the Gulf of Maine," J. Acoust. Soc. Am. **122**, 3003–3004 (2007).
[23]R. C. Dotson and D. A. Griffith, "A high-speed rope trawl for collecting coastal pelagic fishes," California Cooperative Oceanic Fisheries Investigation, Progress Reports **37**, 134–139 (1996).
[24]P. G. Bergmann, "Intensity fluctuations," in *The Physics of Sound in the Sea, Part I: Transmission* (National Defense Research Committee, Washington, DC, 1946).
[25]I. Dyer, "Statistics of sound propagation in the ocean," J. Acoust. Soc. Am. **48**, 337–345 (1970).
[26]N. C. Makris, "The effect of saturated transmission scintillation on ocean acoustic intensity measurements," J. Acoust. Soc. Am. **100**, 769–783 (1996).
[27]M. D. Collins, "A split-step Pade solution for the parabolic equation method," J. Acoust. Soc. Am. **93**, 1736–1742 (1993).
[28]G. Bar-Yehoshua, "Quantifying the effect of dispersion in continental shelf sound propagation," MS thesis, Massachusetts Institute of Technology, Cambridge, MA (2002).
[29]P. Ratilal, Y. Lai, and N. Makris, "Validity of the sonar equation and Babinet's principle for scattering in a stratified medium," J. Acoust. Soc. Am. **112**, 1797–1816 (2002).
[30]M. Andrews, Z. Gong, and P. Ratilal, "High resolution population density imaging of random scatterers with the matched filtered scattered field variance," J. Acoust. Soc. Am. **126**, 1057–1068 (2009).
[31]T. R. Hahn, "Low frequency sound scattering from spherical assemblages of bubbles using effective medium theory," J. Acoust. Soc. Am. **122**, 3252–3267 (2007).
[32]A. Galinde, N. Donabed, M. Andrews, S. Lee, N. C. Makris, and P. Ratilal, "Range-dependent waveguide scattering model calibrated for bottom reverberation in a continental shelf environment," J. Acoust. Soc. Am. **123**, 1270–1281 (2008).
[33]D. Symonds, "Instantaneously imaging and continuously monitoring fish populations over continental-shelf scales using ocean acoustic waveguide remote sensing," Ph.D. thesis, Massachusetts Institute of Technology, Cambridge, MA (2008).
[34]K. G. Foote, "Fish target strengths for use in echo integrator survey," J. Acoust. Soc. Am. **82**, 981–987 (1987).
[35]K. G. Foote, A. Aglen, and O. Nakken, "Measurement of fish target strength with a split-beam echo sounder," J. Acoust. Soc. Am. **80**, 612-621 (1986).
[36]D. N. MacLennan, P. G. Fernandes, and J. Dalen, "A consistent approach to definitions and symbols in fisheries acoustics," ICES J. Mar. Sci. **59**, 365–369 (2002).
[37]E. Ona, "An expanded target-strength relationship for herring," ICES J. Mar. Sci. **60**, 493–499 (2003).
[38]A. P. French, *Vibrations and Waves*, MIT Introductory Physics Series (CRC, Boca Raton, FL, 1971).
[39]F. R. Harden Jones and N. B. Marshall, "The structure and functions of the teleostean swimbladder," Biol. Rev. **28**, 16–83 (1953).
[40]D. N. MacLennan and E. J. Simmonds, *Fisheries Acoustics*, 2nd ed. (Chapman and Hall, London, 1992), pp. 177–182.
[41]F. R. Harden Jones and P. Scholes, "Gas secretion and resorption in the swimbladder of the cod *Gadus morhua*," J. Comp. Physiol. **155**, 319–331 (1985).
[42]O. R. Godø and K. Michalsen, "The use of data storage tags to study cod natural behaviour and availability to abundance surveys in the Barents Sea," International Council for the Exploration of the Sea (1997).
[43]S. M. M. Fässler, P. G. Fernandes, S. I. K. Semple, and A. S. Brierley, "Depth-dependent swimbladder compression in herring *Clupea harengus* observed using magnetic resonance imaging," J. Fish Biol. **74**, 296–303 (2009).
[44]V. M. Brawn, "Physical properties and hydrostatic function of the swimbladder of herring (*Clupea harengus L*)," J. Fish. Res. Board Can. **19**, 635–656 (1962).
[45]J. H. S. Blaxter and R. S. Batty, "The herring swimbladder as a gas reservoir for the acousticolateralis system," J. Mar. Biol. Assoc. U.K. **59**, 1–10 (1979).
[46]J. H. S. Blaxter and J. R. Hunter, "The biology of the Clupeoid fishes," Adv. Mar. Biol. **20**, 1–223 (1982).
[47]J. H. S. Blaxter and R. S. Batty, "The herring swimbladder: Loss and gain of gas," J. Mar. Biol. Assoc. U.K. **64**, 441–459 (1984).
[48]R. E. Thorne and G. L. Thomas, "Acoustic observations of gas-bubble release by Pacific herring *Clupea harengus pallasi*," Can. J. Fish. Aquat. Sci. **47**, 1920–1928 (1990).
[49]G. Sundnes, T. Enns, and P. F. Scholander, "Gas secretion in fishes lacking *rete mirabile*," J. Exp. Biol. **35**, 671–676 (1958).
[50]G. Fahlén, "Morphological aspects on the hydrostatic function of the gas bladder of *Clupea harengus* L.," Acta. Univ. Lund. Sect. II **1**, 1–49 (1967).
[51]R. Fänge, "Gas exchange in fish swim bladder," *Reviews of Physiology Biochemistry and Pharmacology* (Springer-Verlag, Berlin, 1983), Vol. **97**, pp. 111–158.
[52]L. Nøttestad, "Extensive gas bubble release in Norwegian spring-spawning herring (*Clupea harengus*) during predator avoidance," ICES J. Mar. Sci. **55**, 1133–1140 (1998).
[53]G. Fahlén, "Morphology of the gas bladder of *Coregonus laveratus* L.," Acta. Univ. Lund. Sect. II **28**, 1–37 (1967).
[54]G. Sundnes and P. Bratland, "Notes on the gas content and neutral buoyancy in physostome fish," Report on Norwegian Fishery and Marine In-

vestigations **16**, 89–97 (1972).
[55]J. A. Cranston, "Lxi. studies in gas production by bacteria, II. Denitrification and bacterial growth phases," Biochem. J. **24**, 529–548 (1930).
[56]J. S. Link and J. Burnett, "The relationship between stomach contents and maturity state for northwest Atlantic fishes: New paradigms?," J. Fish Biol. **59**, 783–794 (2001).
[57]R. H. Love, "Resonant acoustic scattering by swimbladder-bearing fish," J. Acoust. Soc. Am. **64**, 571–580 (1978).
[58]C. H. Thompson and R. H. Love, "Determination of fish size distributions and aerial densities using broadband, low-frequency measurements," ICES J. Mar. Sci. **53**, 197–201 (1996).
[59]R. W. Nero and M. E. Huster, "Low-frequency acoustic imaging of Pacific salmon on the high seas," Can. J. Fish. Aquat. Sci. **53**, 2513–2523 (1996).
[60]R. W. Nero, C. H. Thompson, and R. H. Love, "Abyssopelagic grenadiers: the probable cause of low-frequency sound scattering at great depths off the Oregon and California coasts," Deep-Sea Res., Part I **44**, 627–645 (1997).
[61]R. W. Nero, C. H. Thompson, and R. H. Love, "Low-frequency acoustic measurements of Pacific hake, merluccicus productus, off the west coast of the United States," Fish. Bull. **96**, 329–343 (1998).
[62]D. Weston, "Sound propagation in the presence of bladder fish," in *Underwater Acoustics*, edited by V. M. Albers (Plenum, New York, 1967), Vol. **2**, pp. 55–88.
[63]Z. Ye, "Low-frequency acoustic scattering by gas-filled prolate spheroids in liquids," J. Acoust. Soc. Am. **101**, 1945–1952 (1997).
[64]C. Feuillade and M. F. Werby, "Resonances of deformed gas bubbles in liquids," J. Acoust. Soc. Am. **96**, 3684–3692 (1994).
[65]E. Ona, "Physiological factors causing natural variations in acoustic target strength of fish," J. Mar. Biol. Assoc. U.K. **70**, 107–127 (1990).
[66]N. Gorska and E. Ona, "Modelling the effect of swimbladder compression on the acoustic backscattering from herring at normal or near-normal dorsal incidences," ICES J. Mar. Sci. **60**, 1381–1391 (2003).
[67]N. C. Makris, P. Ratilal, D. T. Symonds, S. Jagannathan, S. Lee, and R. W. Nero, "Fish population and behavior revealed by instantaneous continental shelf-scale imaging," Materials and methods are available as supporting material on *Science* online (2006).
[68]P. H. Dahl and O. A. Mathisen, "Measurement of fish target strength and associated directivity at high frequencies," J. Acoust. Soc. Am. **73**, 1205–1211 (1983).
[69]A. Leon-Garcia, *Probability and Random Processes for Electrical Engineering*, 2nd ed. (Addison-Wesley Longman, Reading, MA, 1994), p. 288.
[70]H. Bucker, "Sound propagation in a channel with lossy boundaries," J. Acoust. Soc. Am. **48**, 1187–1194 (1970).
[71]S. Gauthier and G. A. Rose, "Target strength of encaged Atlantic redfish (*Sebastes* spp.)," ICES J. Mar. Sci. **58**, 562–568 (2001).
[72]C. Stransky, "Geographic variation of golden redfish (*Sebastes marinus*) and deep-sea redfish (*S. mentella*) in the North Atlantic based on otolith shape analysis," ICES J. Mar. Sci. **62**, 1691–1698 (2005).